Seismically Induced Landsliding in Seattle: A Magnitude 7 Seattle Fault Earthquake Scenario

Kate Allstadt and John Vidale (PI)

15 May 2012

University of Washington
Department of Earth and Space Sciences
Johnson Hall Rm-070, Box 351310
4000 15th Avenue NE
Seattle, WA 98195-1310

allstadt@uw.edu
206-543-0570

vidale@ess.washington.edu
206-543-6790

USGS NEHRP Final Technical Report
Grant Award Number G11AP20012
Award Period: 1 December 2010 – 29 February 2012

Research supported by the U.S. Geological Survey (USGS), Department of the Interior, under USGS award number G11AP20012. The views and conclusions contained in this document are those of the authors and should not be interpreted as necessarily representing the official policies, either expressed or implied, of the U.S. Government.

Abstract

Seattle, Washington is susceptible to both landsliding and large earthquakes, and as a result is prone to seismically induced landsliding, yet this effect has not yet been thoroughly studied. To better understand and quantify the impact triggered landsliding could have on the city, we simulated shallow landsliding for one of Seattle's worst-case scenarios - a magnitude 7 earthquake on the Seattle fault, a shallow crustal thrust fault directly below the city.

Starting with the standard Newmark method, we extend it by generating broadband synthetic seismograms for this specific future event and use those to simulate landslide triggering. The synthetic seismograms we generate account for directivity and basin amplification and are then adjusted for site-specific 1D amplifications in the shallow soil layers, all of which we found to be critical in determining the extent of landsliding triggered. We map relative hazard; we also designate actual slope failures based on the slope displacements (Newmark displacement) calculated for each cell, estimate runout, and look at the intersection between the simulated landslides and infrastructure. We are able to do this analysis on a 5-meter grid because of the wealth of detailed preexisting static slope stability information available.

Our results show that landsliding triggered by a large Seattle fault earthquake will be extensive and potentially devastating, causing both direct losses and impeding recovery. When shallow soils are dry, our simulation predicts about 6,500 landslides within city limits that, along with runout, affect 0.5% of the total land area of Seattle, primarily along steep slopes near the fault south of downtown. This landsliding could affect on the order of 1,000 structures and several kilometers of roads. When soils are completely saturated - a true worst-case scenario - our simulation predicts over 41,000 landslides that, including runout, affects 3% of the city's land area. In both cases, the long period ground motions (<1Hz) are responsible for roughly half the number of triggered slides, but no known research has addressed whether or not shallow landslides are sensitive to longer periods. In any case, our results strongly suggest that seismically induced landsliding in Seattle has the potential to have great human and economic impacts. In order to be more resilient and better prepared, this earthquake effect needs to be much more thoroughly researched and understood.

Table of Contents

Abstract 2

Table of Contents 3

List of Figures 4

List of Tables 4

Introduction 5

Methods 7
- Seismically Induced Landslide Simulation 7
- Determining Slope Failures 9
- Input 1: Slope Stability Information - Critical Acceleration 10
- Input 2: Base synthetic seismograms 11
- Incorporating Site Amplification 14

Validation of Methods 18
- Synthetic Seismograms 18
- Site Amplification Transfer Functions 21
- Seismically Induced Landslide Simulation using Nisqually Ground Motions 21

Results of Mw 7 Seattle Fault Earthquake Simulation 24

Discussion 27
- Particularly Vulnerable Areas and Infrastructure 27
- Comparison with Previously Designated Landslide-prone Areas 29
- Importance of Various Levels of Complexity 30

Conclusions 33
- Future Work 33

Acknowledgements 34

References 35

Map 1 – Newmark Displacements Induced by Mw 7 Seattle Fault Earthquake Scenario – Dry Soil Conditions 40

Map 2 - Newmark Displacements Induced by Mw 7 Seattle Fault Earthquake Scenario – Saturated Soil Conditions 41

Appendix A – Representative Vs profiles 42

List of Figures

1) Map of Seattle showing location of potential sliding areas and location of Seattle Fault
2) Illustration of Newmark Method
3) Probability of failure as a function of Newmark displacement
4) Fault rupture model used to generate broadband synthetics for a M_w 7 Seattle Fault earthquake scenario
5) Example seismograms of broadband synthetics for a M_w 7 Seattle Fault earthquake
6) Peak ground motions of base broadband synthetic seismograms
7) Map of Vs30 values for representative Vs profiles compared with preexisting Vs30 map
8) Peak ground accelerations for broadband synthetic seismograms adjusted for 1D site amplification
9) Validation of broadband synthetic seismograms against NGA attenuation relations
10) Validation of transfer functions generated for representative Vs profiles against spectral ratios for 2001 M_w 6.8 Nisqually earthquake ground motions
11) Validation of representative Vs profiles against measured Vs profiles
12) Map of landslides triggered by simulation using ground motions from M_w 6.8 Nisqually earthquake
13) Map of landslides triggered by simulation of M_w 7 Seattle Fault earthquake
14) Zoom-ins on areas of concern
15) Map of infrastructure intersected by landslides triggered by the M_w 7 Seattle Fault earthquake scenario
16) Dependence of total number of landslides triggered on different levels of simulation complexity
17) Importance of frequency content to the number of landslides triggered

List of Tables

1) Geologic units and engineering properties used to generate representative Vs profiles
2) Results of seismically induced landslide simulation using 2001 M_w 6.8 Nisqually earthquake ground motions
3) Results of seismically induced landslide simulation for the M_w 7 Seattle Fault earthquake scenario
4) Intersections between landslides triggered by the M_w 7 Seattle Fault earthquake scenario and infrastructure
5) Comparison of seismically induced landslides triggered by the M_w 7 Seattle Fault earthquake scenario and relative static landslide hazard designations

Introduction

Seattle's geologic history has left the city with an abundance of unstable slopes and thus frequent landsliding that is exacerbated by a wet climate. When the last ice-sheet receded from the area, it left behind steep slopes composed of unconsolidated soils that were further destabilized in some areas by subsequent wave erosion along coastal bluffs and human activities (Tubbs, 1974).

The two primary natural triggers of landslides in Seattle are water and earthquakes. Triggering by water, primarily by heavy precipitation, occurs most often in Seattle and has been thoroughly studied (e.g. Tubbs, 1974, Harp et al., 2006, Montgomery et al., 2001, Coe et al., 2004, Godt et al., 2006, Laprade et al., 2000). Earthquake-triggered landslides, on the other hand, occur far less frequently and are not as well understood or studied, but landsliding triggered by a major earthquake near the city could potentially have disastrous consequences. Shallow landsliding could be widespread - blocking roads, damaging structures, and cutting off waterlines, sewer, electricity and other lifelines necessary for rescue operations and recovery. This disruption would be concurrent with other primary and secondary hazards of shaking such as liquefaction, building damage and collapse, fires and so on. In addition, large deep-seated translational and rotational slides and submarine landslides could occur with extended shaking (Keefer, 1984), with the potential to impact large areas of the city. In many historical earthquakes worldwide, landsliding caused more human and economic losses than other earthquake effects (Keefer, 2002).

Geologic evidence suggests that widespread catastrophic landsliding triggered by earthquakes has occurred many times in Seattle prior to western settlement (Logan et al, 1998; Pringle et al, 1998, Karlin et al., 2004). Seismically induced landslides are even featured in Salish oral traditions (Ludwin et al., 2005). Known remains of slides triggered by past earthquakes include sunken forests on large block landslides and lake-wide turbidite layers, both found preserved in the depths of Lake Washington (Jacoby et al., 1992, Karlin and Abella, 1992). These deposits have been tied to seven different earthquakes in the last 3500 years (Karlin et al., 2004). It is hard to imagine the consequences of such dramatic landsliding if it occurred today: the areas from which many of those landslides originated are now densely populated.

Modern examples of seismically induced landsliding in Seattle are less numerous because the city has so far evaded its most dangerous seismic sources: subduction megaquakes and large shallow crustal earthquakes. Even so, more than 14 moderate historical earthquakes have triggered landsliding since 1872 (Chleborad and Schuster, 1998, Noson et al, 1988, Keefer, 1983, Hopper, 1981). The three major historical Puget Sound earthquakes, all deep Benioff zone earthquakes (M7.1 in 1949, M6.5 in 1965 and M6.8 in 2001), caused ground failures throughout western Washington and northern Oregon (Chleborad and Schuster, 1998, Highland, 2003), but less than they could have triggered because of the relatively moderate ground motions and lower than normal preceding rainfall in all three cases (Stewart, 2005), which is a main factor in ground stability.

While there are many crustal faults in the Puget Lowland, as well as the Cascadia megathrust fault offshore, the fault that most directly threatens Seattle is the Seattle Fault. The Seattle

fault is a zone of south-dipping reverse faults that runs east-west across the Puget Lowland just south of Downtown Seattle (**Figure 1**). It forms the southern boundary of the sedimentary basin called the Seattle basin upon which most of the city is built (Blakely et al., 2000). Paleoseismic studies have dated the last earthquake on this fault to 900A.D. (Bucknam et al., 1992) with an estimated magnitude around 7.5 (ten Brink et al., 2006). This event triggered some of the landslides preserved in Lake Washington, rock avalanches in the Olympic Mountains (Jacoby et al., 1992, Karlin and Abella, 1992, Karlin et al., 2004, Schuster et al., 1992), and likely much more landsliding than we know about. If the 900 A.D. event is characteristic, the next event could be thousands of years away (Johnson et al, 1999, Pratt et al., 1997), but trenching of a backthrust to the Seattle Fault suggests past recurrence intervals of earthquakes on the fault have ranged from 200 to 12,000 years (Nelson et al., 2003) and glacial loading and unloading could have disturbed the cycle (Thorson, 1996). Therefore the recurrence interval is uncertain.

Despite the evidence, no one has thoroughly studied the potential for seismically induced landsliding in Seattle and the hazards it poses to the city during future earthquakes. There are some reports on past seismically induced landsliding in the area and qualitative studies on the types of soils that failed and thus roughly the areas and soil types that may be prone in the future (e.g. Chleborad and Schuster, 1998, Noson et al, 1988, Keefer, 1983, Hopper, 1981, Stewart, 2005), but so far none address the specifics we need in order to know what to expect and be prepared for: How many landslides should we expect? Where will they be and how far will the runout travel? What if the earthquake happens when soils are saturated? Are there buildings that are at risk and how will important infrastructure such as waterlines, sewer and electricity be impacted? What key transit routes could be obstructed? These are the questions we sought to address in the present study.

Due to the limited timescale of the project, we focused on a scenario study of shallow landsliding triggered by a magnitude 7 Seattle Fault earthquake. Shallow landsliding is defined as having a failure plane less than a few meters deep and would primarily fall into the category of disrupted soil slides as defined by Keefer (1984). Based on regressions of landslide distributions from forty historical worldwide earthquakes that triggered landsliding, a typical magnitude 7 earthquake might trigger around 5,000 landslides over an area of about 3,500 km^2, up to around 150 km from the rupture zone, but most within a few kilometers, and these would primarily be shallow landslides of the type we model in this project (Keefer, 2002). However, there is wide variability dependent on the specifics of each earthquake and the geology of the surrounding areas.

To simulate landsliding, we use methods often used to study regional seismically induced landslide hazard, a modification of the Newmark method developed by Jibson et al., (2000). The primary difference between this study and previous studies is that we generate broadband synthetic seismograms adjusted for site-specific amplification to use as the ground motion input, while previous studies either use recordings of past earthquakes or a simplified ground motion parameter such as Arias intensity or peak ground acceleration. We also turn this into a scenario study, by designating cells that fail and estimating the runout in order to look at infrastructure vulnerability, rather than just looking at relative hazard. Furthermore, we are able to do this study on a finer scale for Seattle than in other areas because of the detailed slope stability work done by Harp et al. (2006).

In this report, we first present the methods we developed for the seismically induced landslide simulation, the next section details how we validated the methods. This is followed by the results of our seismically induced landslide simulation of a magnitude 7 Seattle fault earthquake for both dry and saturated soil conditions and a discussion of the patterns and extent of landsliding and potential impacts on infrastructure. Finally we conclude and discuss what needs to be done next.

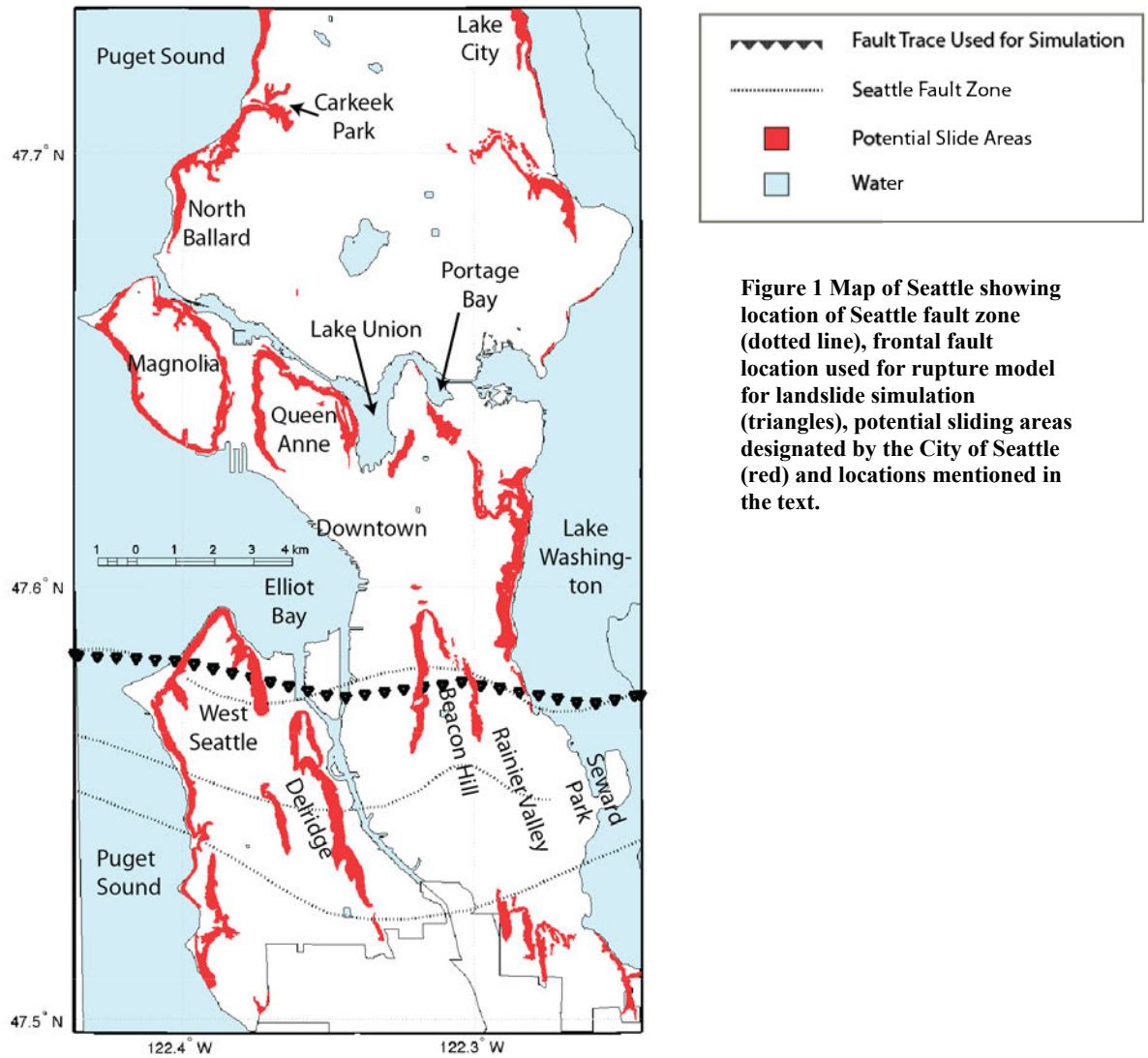

Figure 1 Map of Seattle showing location of Seattle fault zone (dotted line), frontal fault location used for rupture model for landslide simulation (triangles), potential sliding areas designated by the City of Seattle (red) and locations mentioned in the text.

Methods

Seismically Induced Landslide Simulation

Newmark Method

The core of the seismically induced landslide simulation we use is a modification of the Newmark Method (Newmark, 1965), a method originally developed for estimating seismic displacements of manmade earthen dams by approximating a slope as a rigid friction block

sliding down an inclined plane. Though the model is not a realistic representation of natural slopes, with a few modifications, it is currently one of the most widely used tools for looking at the susceptibility of natural slopes to landsliding triggered by earthquakes.

Jibson et al. (2000) modified the Newmark method for use in regional assessments of seismically induced landslides. We use a similar approach in this study. The study area, the city limits of Seattle, is discretized into 5-meter cells (**Figure 2a**). Each cell is approximated as a rigid block held by friction on a ramp that has an incline equal to the average slope within that cell (**Figure 2b**). The block initially is stable and does not slide down the ramp, but when an earthquake shakes the system, there is a threshold ground acceleration in the downslope direction above which the block starts to slide down the ramp. This value is known as the critical acceleration (a_c), sometimes referred to as the yield acceleration. The block accumulates displacement down the ramp as the shaking progresses each time the critical acceleration is exceeded. The final displacement, referred to as the Newmark displacement, is calculated by integrating the portions of the accelerogram that exceed the critical acceleration in the down-slope direction twice to obtain displacement (**Figure 2c**). Note that after integrating once to velocity, in order to bring the velocity back to zero when the acceleration drops back below the critical acceleration after each exceedance, we assume a symmetrical pulse shape. In order to speed up calculations, we only calculate Newmark displacement for slopes equal to or greater than 10°. We also do not calculate Newmark displacement for slopes greater than 64° because only manmade structures are that steep at the resolution of our slope map (5m).

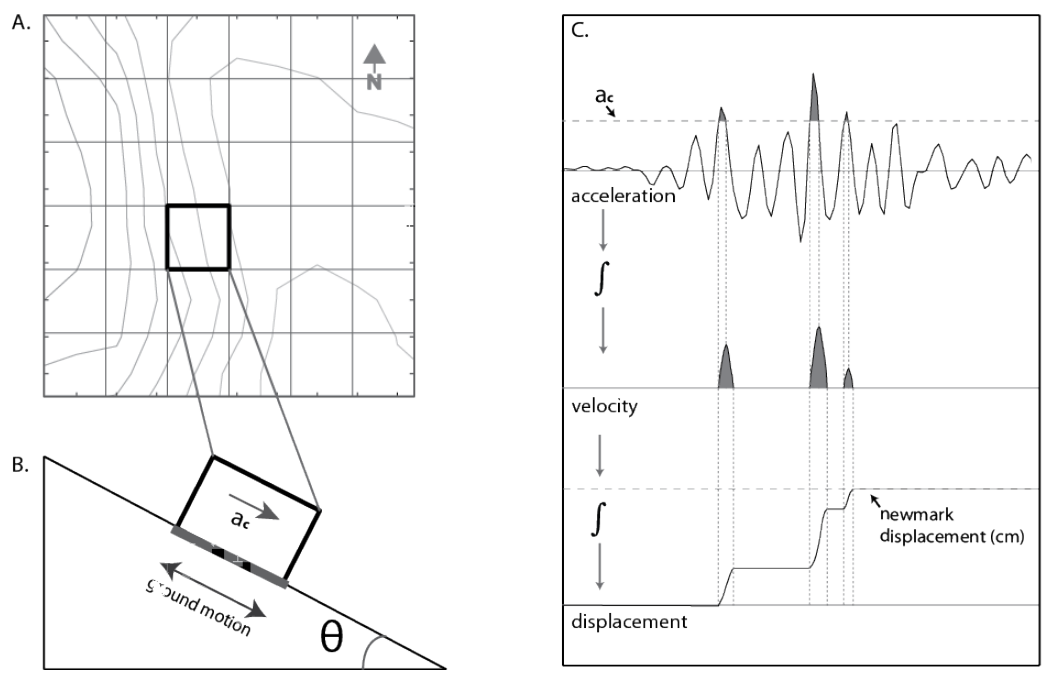

Figure 2 Illustration of digital Newmark method. A) The study area is discretized into cells B) Each cell is approximated as a block sliding down a ramp with an average slope of θ that has a critical acceleration (a_c) dependent on soil properties and slope. When ground acceleration exceeds a_c the block begins to accumulate displacement as it moves down the ramp. C) To calculate the final displacement, the slope parallel acceleration that exceeds a_c in the downslope direction (top) is integrated to velocity, assuming a symmetrical shape for each velocity pulse to bring velocity back to zero after each exceedance of a_c (middle) and then integrated to displacement. The final accumulated displacement is the Newmark displacement (bottom) that corresponds to the likelihood that the natural slope represented by each cell will fail in a landslide.

Determining Slope Failures

For natural slopes, the final Newmark displacement does not correspond to the actual distance a landslide will move downslope, but rather the likelihood a landslide will be triggered in that cell when it is subjected to the specified ground motion. It can be used as a marker of relative likelihood of landsliding, as in Jibson and Michael (2009), but for this scenario study we choose cells that "fail" and become landslide sources. Rather than choosing a single threshold of 10 to 15cm (as in Wieczorek et al., 1985 or Keefer and Wilson, 1989), which would result in every single unstable cell failing – which is not likely due to natural variability beyond our observation abilities - we take a probabilistic approach. Jibson et al. (2000) developed a probability curve to relate Newmark displacement to the probability of failure developed using the landslide distribution triggered by the magnitude 6.7 Northridge Earthquake in Southern California in 1994. The data showed that the probability maxed out around 34% at 18cm displacement (**Figure 3**), which is considered catastrophic failure on natural slopes. This is the only such probability curve developed so far because of the lack of comprehensive earthquake-triggered landslide surveys in areas with dense ground motion recordings.

The moist unconsolidated soils that compose most of Seattle may be compliant and able to tolerate more displacement than the brittle rocks and dry soils of Southern California so the probability curve developed for the Northridge earthquake may overestimate the number of landslides in Seattle, but still predicts far fewer than if we chose a set threshold displacement. As we do not know of any research that might guide us on how to modify the probability curve to better suit Seattle, for this study we use the Northridge curve as is to determine the probability of failure of each cell on the 5m-grid throughout the city. Then, using a random number generator, we determine if each cell fails or not based on its probability of failure.

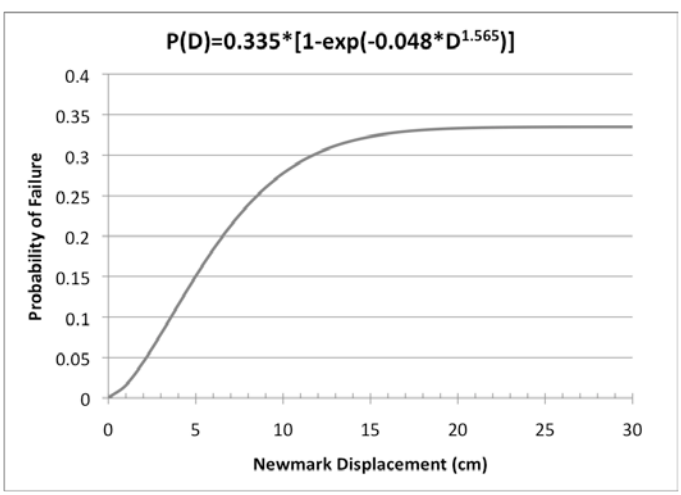

Figure 3 This curve and equation relates the Newmark displacement (D) of a given cell to its probability of failure P(D). The relation is based on the landslide distribution of the Northridge earthquake (Jibson et al., 2000).

Failure is defined as a detachment of the slope that turns into a gravity-driven rapid landslide. These will primarily be "disrupted soil slides" as defined in Keefer (1984, 2002). The failure of each cell is independent of all the others. The exact distribution of landslides changes each time the landslide simulation model is run because of the dependence on a random number

generator to define failures, but the overall patterns remain the same. Once the distribution of failed cells throughout the city is determined, adjacent failed cells are clustered together into landslide source areas. Each cluster of adjacent failed cells is counted as one source.

Estimation of Runout

Landslide damage can occur both in the source area and the runout, which can cover a greater area. We estimate runout from each failed cell using empirical methods based on the travel distance angle - the slope of a straight line drawn between the source area and the end of debris deposition. We use the methods developed by Hunter and Fell (2003) for unconfined failures in natural slopes with dilative soils:

Equation 1

$$H/L = 0.77\tan\theta + 0.087$$

Where H is the drop in elevation, L is the horizontal distance traveled, and θ is the angle of the slope of the surface over which the material is flowing. The calculation of runout distance occurs in two steps. For the first step, starting at the source cell, the material is allowed to flow downhill, and H/L is calculated as the flow arrives at each new cell until it reaches the mean value of H/L for the slides in the database used by Hunter and Fell (2003). For the type of slopes we are interested in - unconfined failures in natural slopes with dilative soils - the mean H/L is 0.547. This first rough estimate of the runout is used to obtain the mean slope of the surface over which the material flows, θ. Then, in the second iteration, the value of θ is plugged into **Equation 1** and again the material is allowed to flow downhill, calculating H/L at each step until it reaches the point where H/L equals the right side of **Equation 1**. Note that the landslide runout data used by Hunter and Fell (2003) to derive this equation most likely come from landslides with higher water content than seismically triggered landslides in dry soil conditions, so runout may be overestimated in the dry soil scenarios.

Input 1: Slope Stability Information - Critical Acceleration

Slope stability information is a critical input to the regional Newmark method. Fortunately Harp et al., (2006) conducted a detailed study of slope stability in Seattle. For this study they calculated the factor of safety for dry and completely saturated soil conditions on a 2-meter grid for the entire city using typical engineering properties for each geologic unit. The factor of safety is the ratio of resisting forces to driving forces. A factor of safety less than 1 means the slope is unstable. Harp et al. (2006) calculated the factor of safety for a uniform failure thickness of 2.4 meters to simulate shallow landslides of the same type we are investigating in this project. For dry conditions, they set the saturated thickness to zero, and it was set to be the entire failure thickness for saturated conditions meaning the water table is essentially at the surface. The results of the seismically induced landslide simulation calculated using the factor of safety for saturated conditions represents a highly unlikely worst-case scenario where an extreme storm event brings hours or days of heavy precipitation to the area with an already high water table, and then an earthquake strikes. The scenario referred to as “dry conditions,” where the top 2.4 meters of the subsurface are moist but not saturated, is a much more likely scenario.

The factor of safety (FS) and slope angle (θ) of each cell can be used to calculate the critical acceleration (a_c), which is the acceleration in the downslope direction required to reduce the factor of safety to 1:

Equation 2

$$a_c = (FS - 1) g \sin\theta$$

where g is the acceleration due to gravity. High-resolution slope information (1.83-meter resolution) was available from the Puget Sound LIDAR Consortium.

Because the factor of safety was calculated on a regional scale using a simple model, the factor of safety reported by Harp et al., (2006) was less than 1 for some cells under dry soil conditions, and for many cells for wet conditions, meaning the cell should have already failed even without the help of the ground shaking. This would result in the maximum possible accumulation of Newmark displacement in our simulation - the entire positive area under the seismogram. To look at only landslides triggered by ground motion, we assume that prior to the earthquake, all land is at least marginally stable so we raise all cells with factors of safety below 1 to 1.01.

Input 2: Base synthetic seismograms

The most important input to the Newmark method is the ground acceleration, but of course we don't have actual recordings of a large earthquake on the Seattle fault because it has not occurred since the invention of modern seismometers. Because of this predicament, previous studies of seismically induced landsliding tend to use simplified ground motion parameters such as Arias Intensity or peak ground acceleration that can be obtained by ground motion prediction equations in combination with regression equations to estimate Newmark displacement from those parameters (such as Jibson, 2007), all of which introduces a lot of uncertainty. However, we can do much better in Seattle. Delorey and Vidale (2010) developed a 3D velocity model of the Seattle basin using the noise correlation of Rayleigh waves. Using this with a finite-difference code developed by Liu and Archuleta (2002) we generate deterministic seismograms with frequency content accurately represented at frequencies up to 1Hz. We then combine the deterministic portion with stochastic higher frequency ground motion using methods developed by Frankel (2009) to generate broadband synthetic seismograms. Synthetic seismograms have the benefit of accounting for directivity effects, basin amplification, duration, and spatial variation.

Magnitude 7 Seattle Fault Earthquake

We chose to simulate a magnitude 7 earthquake for the scenario as a compromise between the estimated maximum magnitude the fault is capable of generating: M7.6 to 7.7 (Pratt et al., 1997), and the size of the earthquake that could be generated by the estimated slip accumulated since the last earthquake on the main fault, 75 to 120cm (Johnson et al, 1999), capable of producing, on average, a magnitude 6.5 earthquake (Wells and Coppersmith, 1994).

Rupture Model

For the rupture plane of the simulation, we use the surface projection of the frontal fault (**Figure 4A**) from Blakely et al. (2002) dipping 45 degrees to the south. We rupture a 45 km segment from the middle section of the fault and constrain it to be seismogenic from 3km to

15km. While slip most likely occurs higher on the fault as well, it probably does not release significant seismic energy, and we found if we allowed the fault to rupture above 3km depth in our simulation it produced unrealistically high ground motions.

The rupture plane is divided into 3150 subevents spaced 500 meters apart that have a mean moment magnitude of 4.6 (**Figure 4B**). Using methods developed by Frankel et al. (2007) we model the slip distribution, and thus the moment distribution, among the subevents as a spatial random field with a correlation length corresponding to the magnitude of the earthquake (Mai and Beroza, 2002).

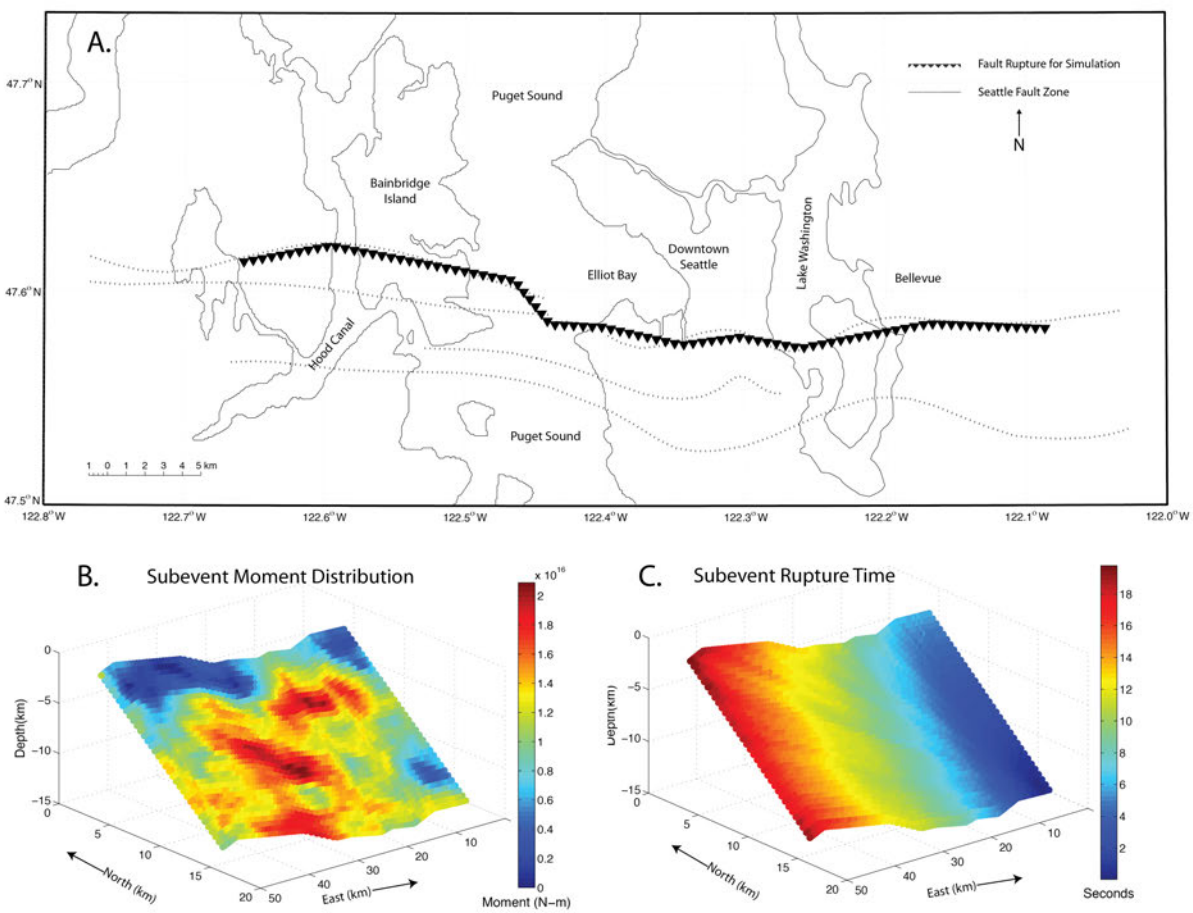

Figure 4 A) The surface projection of fault rupture used to generate synthetic seismograms is plotted with triangles and corresponds to the frontal fault of the Seattle Fault Zone (Blakely et al, 2002). The entire Seattle Zone is shown by the gray dotted line. B) The fault surface used in the simulation dips at 45 degrees to the south and is divided into 3150 subevents with an average moment magnitude of 4.6. The patches of higher moment have a correlation distance corresponding to the magnitude of the full earthquake (Mai and Beroza, 2002). C) Rupture propagation was started at the lower eastern edge of the fault zone and propagates westward. Rupture velocity between adjacent subevents is initially set to 70% of the shear wave velocity at that depth and then randomized by 25% but constrained to never exceed the shear wave velocity.

To simulate a finite fault rupture, the point source subevents start rupturing first at the lower eastern edge of the fault and propagate updip and westward at rupture velocity. Rupture velocity is set to 70% of the shear wave velocity, so that it becomes slower as the rupture

approaches the surface, and is randomized by 25% and constrained to never exceed the shear wave velocity in order to avoid unrealistic directivity pulses (**Figure 4C**). In addition, the rake of each subevent varies randomly by ±20°. The rise time (T_D) for each subevent depends on rupture velocity (β) at the source, and the geometry of the fault (Stein and Wysession, 2003):

Equation 3

$$T_D = 16Lf^{0.5}/(7\beta\pi^{1.5})$$

Where L is the length of the fault and f is the ratio of width to length. Because Equation 3 depends on the shear wave velocity, shallower subevents have longer rise times than deeper ones. We then use this fault rupture model to generate broadband seismograms, calculating long period motion (<1Hz) deterministically, high frequency motion (>1Hz) stochastically, and combining them using methods developed by Frankel (2009).

Low frequencies (<1 Hz)

Long period motion, including directivity pulses and basin amplification, can be calculated deterministically. We used the fault rupture model shown in Figure 4 as input to a finite-difference code developed by Liu and Archuleta (2002) to propagate waves through a 3D velocity model of the Seattle basin developed by Delorey and Vidale (2010) that will simulate basin amplification. We also generate synthetic seismograms using a 1D velocity model based on the out-of-basin velocities in Delorey and Vidale's (2010) 3D model to constrain the influence of the Seattle basin on ground motions and consequently on the extent of landsliding triggered. Both velocity models have a base shear-wave velocity of 600 m/s at the surface.

High frequencies (>1 Hz)

Due to computational limitations and a lack of knowledge of shear wave velocity on the scale required, higher frequency portions of the seismogram were computed stochastically using the constant stress-drop model proposed by Frankel (2009), derived from methods developed by Boore (1983, 1996), and modified to suit Seattle geology. Subevents were assigned stress drops using a fractal distribution with a root mean square value of 100 bars. This was used to calculate a theoretical spectrum for each event, which is then multiplied by Gaussian white noise in the frequency domain so that each subevent has a realistic seismogram when transformed into the time domain. These are then adjusted for attenuation, geometrical spreading, and travel times between each source and each station and added up as each subevent ruptures with the timing shown on Figure 4.

Broadband Seismograms

The high and low frequency synthetics were generated on a 210-meter grid throughout the city and combined at 1Hz to form broadband seismograms. Some sample seismograms are shown on **Figure 5** and the maximum peak ground accelerations for this earthquake in the vertical and horizontal directions for the 3D velocity model and the 1D velocity model are shown on **Figure 6**. This is a randomized iteration of a possible Seattle Fault earthquake and only represents one possible scenario. Peak ground accelerations will vary with each iteration, but the general pattern will likely remain the same: the hanging wall will experience the highest accelerations because it is closest to the fault and the shaking will be much lighter in the northern parts of the city.

The 3D velocity model that accounts for the Seattle basin generates higher peak ground accelerations and more spatial variability within the basin north of the Seattle fault because of basin amplification effects. Peak ground accelerations are higher in the northwest corner in particular due to amplification along the northern edge of the Seattle basin.

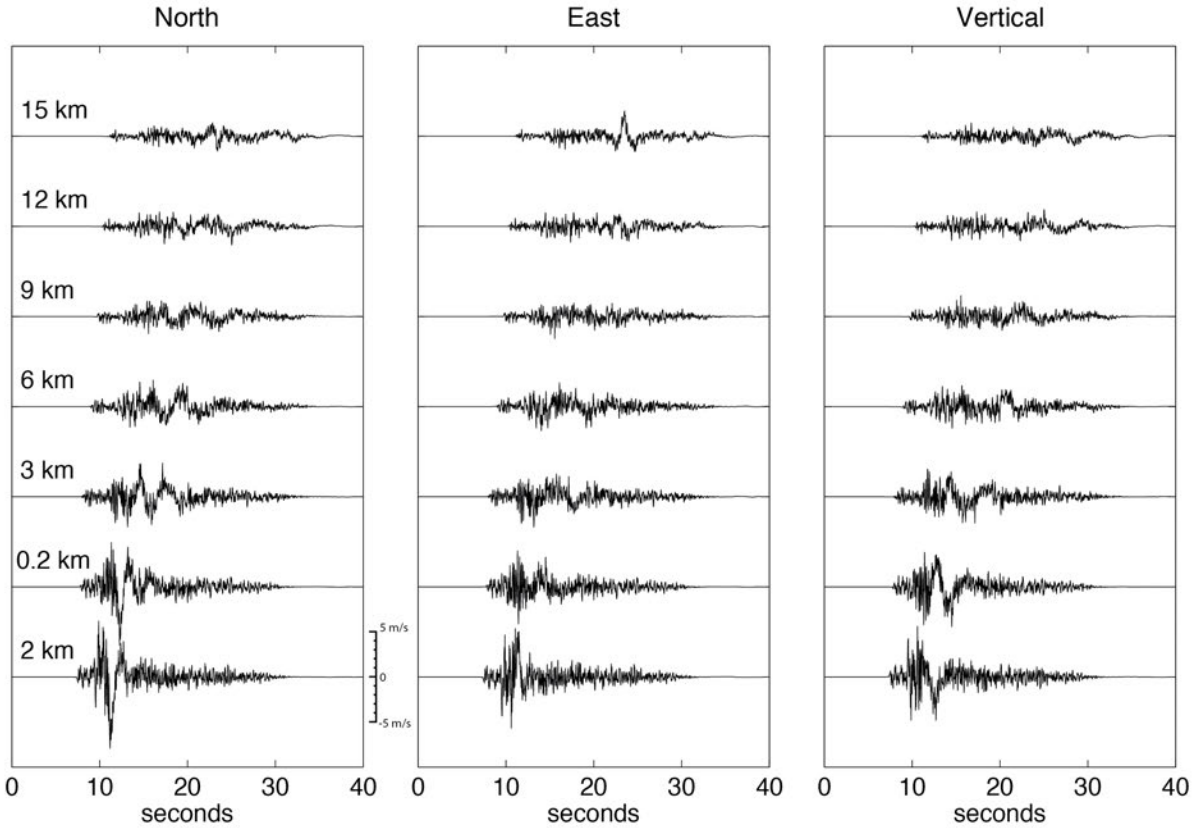

Figure 5 Example North, East, and Vertical seismograms starting from south of the surface trace of the fault at bottom, moving northward toward the top of the plot. Distance to the closest point on the frontal fault trace is shown to the left of each seismogram. Locations of each seismogram are shown on Figure 6.

Incorporating Site Amplification

The broadband seismograms we generated represent shaking at the surface with a base shear wave velocity of 600 m/s. Most of the city is underlain by layers of soil with much lower shear wave velocities near the surface that can amplify ground motion (Pratt and Brocher, 2006, Frankel et al., 2002, Pratt et al., 2003, Pratt and Brocher, 2006, Snelson et al., 2007, Hartzell et al., 2000). In order to simulate realistic ground motions, we need to account for site amplification relative to the 600 m/s base layer used to generate the synthetics. No effective simple methods yet exist for adjusting a full seismogram in the Fourier domain for site effects on a regional scale, so we developed our own site amplification transfer functions for representative units defined throughout Seattle.

Development of representative shear wave profiles

We developed 67 representative shear wave (Vs) profiles that represent the spectrum of typical geologic profiles found in Seattle. These are based on the new "Geologic Map of Seattle" and its cross-sections and typical thicknesses listed for each unit (Troost et al., 2005), typical

engineering properties, typical shear wave velocity ranges, and actual measured shear wave profiles for these units reported in Savage et al. (2000), Williams et al. (1999), Wong et al. (2010), and Palmer et al. (2004). The geologic units and the range of engineering properties we used to construct these representative profiles are shown in **Table 1** and complete profiles are included in **Appendix A**. For simplicity, all unconsolidated deposits older than the last glaciation (Vashon stade of Fraser glaciation) are lumped together as Qpf. These units are nearly all classified as very dense and hard, and have been overconsolidated by one or more glaciations so they are assumed to be equivalent to the base layer of 600 m/s, with a transition from 400 to 600 m/s for deposits that are near the surface. Soils of this site class (NEHRP class C) do not show much non-linear behavior (Choi and Stewart, 2002), so we assume they behave linearly. The only rock sites in the entire city are a few soft rock sites in the southern portion of the city. We also assume these behave linearly and have a shear wave velocity of 600 m/s, with a transition near the surface to account for weathering and shallow soil coverage.

Table 1 Description of Units used in the development of the representative Vs profiles and the range of thicknesses and engineering properties they were assigned. Naming convention from Troost and Booth (2008).

Unit	Typical Thickness range (m)	Vs range (m/s)	Wet density range (kg/m^3)	Description	Age
Qvt	8	400-600	2160-2400	Vashon Till	Fraser Glaciation Vashon Stade (pleistocene)
Qva	10-50	300-600	1920-2160	Advance Outwash Deposits	
Qvr	5	250-350	1680-1800	Recessional Outwash Deposits	
Qvrl	5	250-350	1560-1800	Recessional Lacustrine Deposits	
Qvlc	15-30	200-500	1560-1920	Lawton Clay	
Qpf	NA	450-600	2160-2400	Pre-fraser Deposits	pleistocene
Tb	NA	350-600	2300-2400	Blakely Formation (weakly lithified sandstone)	Tertiary
soil	1	100	1440	Soil	postglacial (holocene)
Qp	10	60	1260	Peat	
Qal	6-30	120-180	1440-1620	Alluvium	
Qt	6	120-130	1440	Terrace deposits	
Qls	3-10	120-140	1440-1500	Landslide deposits	
Fill	2-10	120-140	1440-1500	Artificial Fill	
Qb	8	120-140	1440-1500	Beach	
Ql	3	130-150	1560-1680	Lake Deposits	

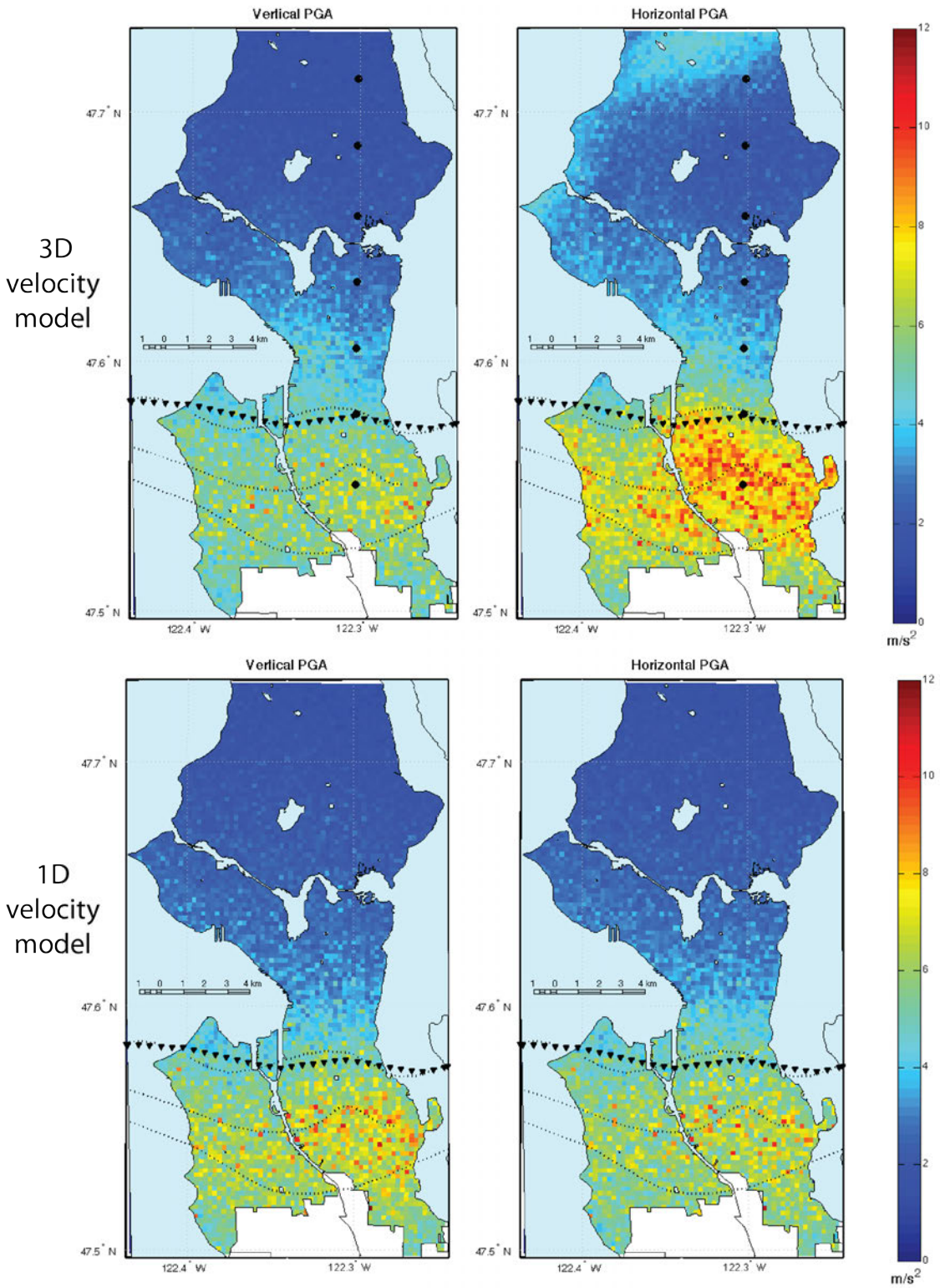

Figure 6 Vertical and horizontal peak ground accelerations in m/s^2 of broadband synthetic seismograms of the simulated Mw 7 Seattle fault earthquake generated using a 3D velocity model (Delorey and Vidale, 2010) that simulates 3D basin amplification (top) compared to synthetic seismograms for the same rupture model generated using a 1D velocity model of the Puget Lowland outside the Seattle basin. The graininess is due to the cell size of 210-meters. Triangles delineate the rupture used to generate seismograms, dotted lines show the Seattle fault zone.

Figure 7 shows the average shear wave velocity in the top 30 meters (Vs30) calculated from these profiles, compared to the existing Vs30 map for Seattle that was done on a much coarser scale by Palmer et al. (2004). Overall the two are similar, with most areas having Vs30 values ranging from 300 to 450 m/s. In the northeast section of Seattle our representative profiles have higher Vs30's because we have accounted for the fact that the pre-Vashon (Qpf) deposits are closer to the surface in the East. Palmer et al. (2004) has higher velocities at the top of the hills in the western and middle section of North Seattle, where our model has lower Vs30's because we have accounted for the underlying thicker layer of advance outwash. Palmer et al., (2004) also has a larger area classified as rock, the Blakely formation, in southeastern Seattle, and assigns much higher velocities than we do. However, the Vs profiles measured at sites there in Seward park (Wong et al., 2010, Williams et al., 1999) show much lower Vs30's than Palmer et al., (2004) reports for that area because of the presence of soil and weathered bedrock over the weakly lithified Blakely formation. We concentrated our efforts in the development of these profiles on areas that could generate landslides. Consequently, profiles for flat-lying areas, such as the Duwamish valley, Harbor Island, and Interbay, are oversimplified.

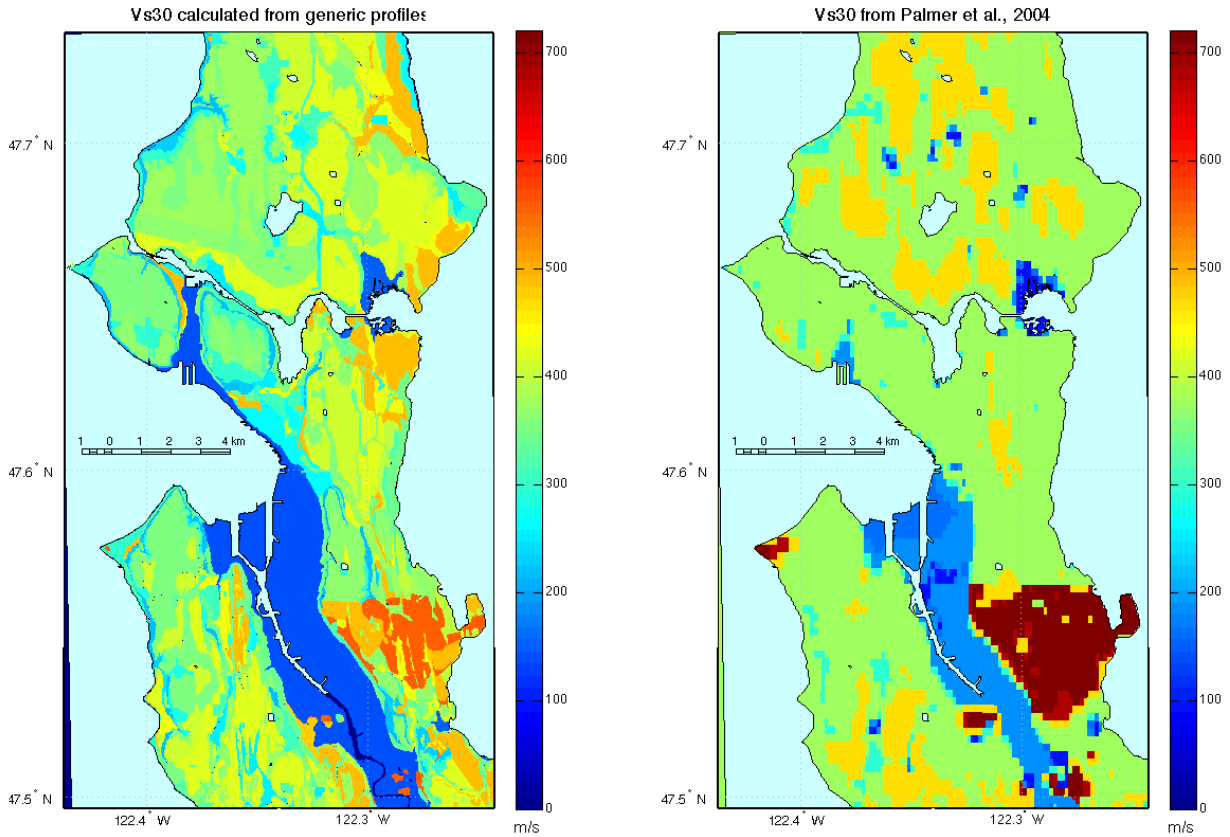

Figure 7 Average shear wave velocity down to 30 meters (Vs30) in m/s for representative profiles calculated for this project (left) compared to values on the pre-existing regional Vs30 map developed by Palmer et al. (2004) (right).

1D Site Amplification Transfer Functions

In order to obtain site amplification transfer functions for these representative 1D Vs profiles, we input them to the 1D equivalent linear ground response analysis software, ProShake, using a representative broadband synthetic seismogram that we generated for the M_w 7 Seattle fault

event as the input ground motion. The program outputs Fourier spectrum transfer functions of 1D site amplification for shear waves that approximates non-linear effects using an equivalent linear approach.

Topographic Amplification

Amplification at the crests of hills and de-amplification at the base has been observed in many earthquakes and can be an influential factor to the occurrence of seismically induced landslides (e.g. Harp and Jibson, 2002, Peng et al., 2009a,b). People have been working for decades on various analytical, numerical, and empirical methods of calculating topographic amplification (e.g. Aki and Larner, 1970, Boore, 1972, Bard and Tucker,1985, Geli et al., 1988, Ashford et al., 1997, Paolucci, 2002). None of these have reproduced observations very well because it is hard to decouple topographic effects from other site effects and the areas where topographic amplification is most important are often geologically complex; however many match qualitatively and get the frequencies right (Geli et al, 1988). Using numerical methods was beyond the scope and computing power available for the current project. Instead, we estimated topographic amplification using an analytic solution of the amplification of SH-waves on a simple wedge (Sanchez-Sesma, 1985). Seattle is made up primarily of north-south oriented elongated ridges. When sliced east-west they can be approximated as simple wedges. However, because the ridges are much wider than they are tall, the wedge angles turned out to be close to 180 degrees in some cases, and thus the maximum amplification we found on the scale of these topographic features was 1.04. Such a small amplification is essentially insignificant and made virtually no difference to the results. We did not compute topographic amplification on finer-scaled features because they could not be well approximated as a wedge, but topographic amplification could be more significant on a finer scale or along the edges of bluffs and should be investigated further in future work.

Peak Ground Accelerations adjusted for Site Amplification

We apply the corresponding transfer functions to the base seismogram for each 5-meter cell prior to calculating Newmark displacement. **Figure 8** shows the horizontal peak ground accelerations before and after the transfer functions are applied to each unit. The ground motion in some areas is deamplified due to soil non-linearity, particularly areas of fill and alluvium, where liquefaction will be more of an issue. Areas that are amplified relative to their surroundings include old landslide deposits along many of the steep coastal bluffs, and areas where thin lower velocity deposits like recessional outwash or soil overlie pre-Vashon deposits or soft rock sites that behave linearly. The soft rock sites have a higher Vs30 than much of the city, yet also have some of the highest amplifications, indicating that Vs30 may not be the best indicator of site response. Accelerations reach 2g's in a few of these localized areas on the hanging wall of the fault.

Validation of Methods

Synthetic Seismograms

To validate the broadband synthetic seismograms, we calculated their spectral accelerations (response spectra for 5% critical damping) and compared them to the spectral accelerations predicted for a magnitude 7 thrust fault earthquake by three of the Next Generation Attenuation (NGA) relations. The NGA relations are ground motion prediction equations that

are derived from actual earthquake recordings. They output response spectra, which shows the "spectral acceleration" of a single degree of freedom system of a range of fundamental periods in response to the input ground motion. Shahi and Baker (2010) developed a modification to the attenuation relations that accounts for a directivity pulse. The broadband synthetics we generated have a directivity pulse, primarily on the fault-normal (North) component, because of the updip rupture, so we include their modification to the NGA relations for fault-normal components (~North). **Figure 9** shows the response spectra calculated for the synthetics we generated with a base shear wave velocity of 600 m/s (NEHRP Class C site). We calculate response spectra for each station and bin them in 2km wide bins based on the closest distance to the fault.

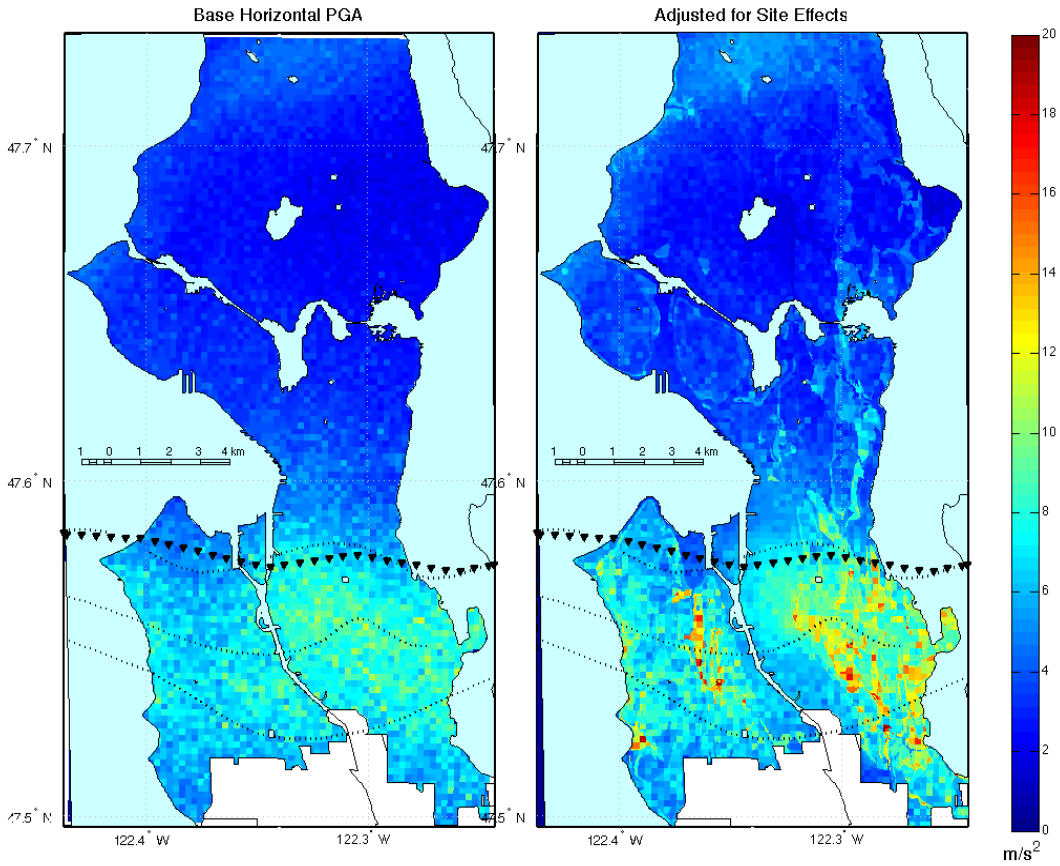

Figure 8 Maximum horizontal peak ground acceleration in meters per second for the base synthetic seismograms generated using the 3D basin velocity model with a surface layer of 600 m/s at left and the same seismograms adjusted for 1D site amplification due to the shallow surficial soil layers and topographic amplification at right.

The mean spectral acceleration of the synthetics for the distance to the fault labeled at the top of each plot ± 1km is shown on **Figure 9**, with one standard deviation denoted by the error bars. This is compared with the spectra for three NGA relations and the mean of all three together. The top figure shows the response spectra for synthetics generated with the 3D basin velocity model and the bottom shows the synthetics generated using a 1D velocity model. The fit is quite good, particularly taking into account the large variability between the NGA attenuation relations themselves and their respective uncertainties, and the spatial variability within the synthetics as shown by the error bars. For periods shorter than 1 second

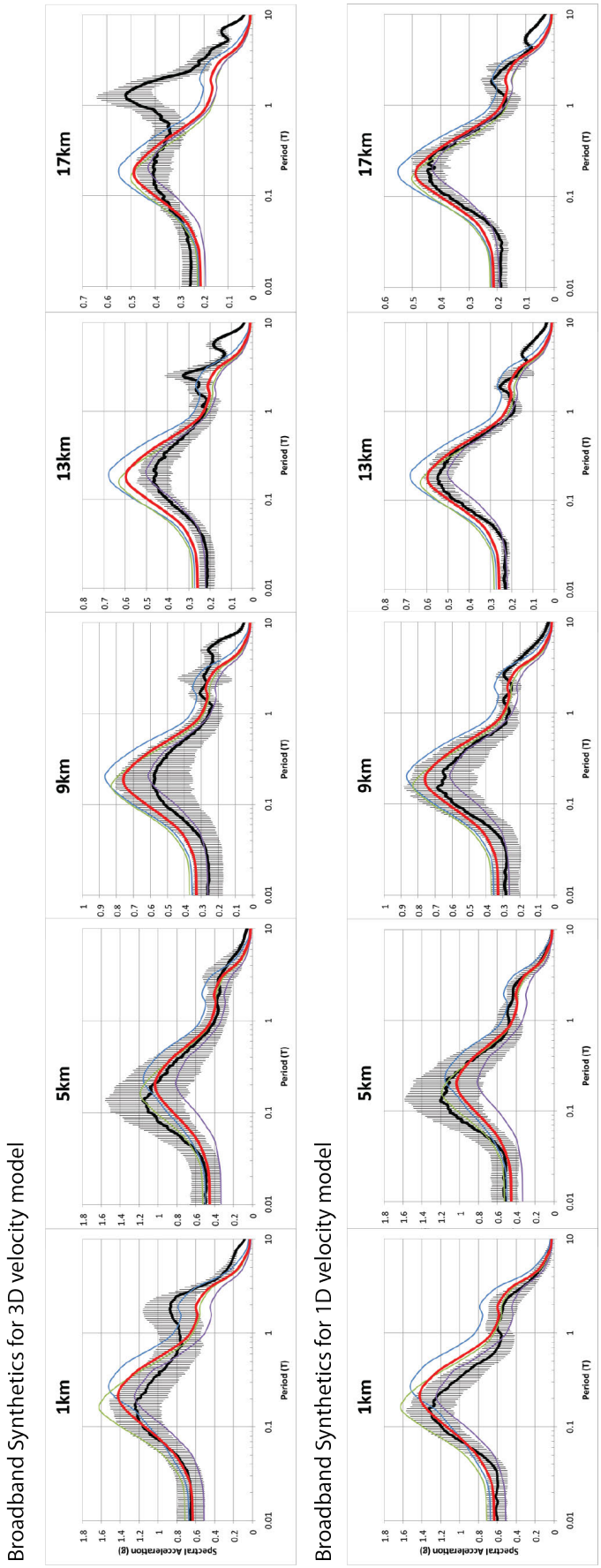

Figure 9 Response spectra for 5% critical damping of the broadband synthetics generated with the 3D basin velocity model (top) and the 1D basin model (bottom) compared with the mean values for three Next Generation Attenuation relations and modified to include a directivity pulse using methods developed by Shahi and Baker (2010). Black is the mean of the synthetics at the distance bin noted ±1km with one standard deviation indicated by the error bars. Red is the mean of the three attenuation relations, blue is the response spectra for Campbell and Borzorgnia (2008), green is Chiou and Youngs (2008), and purple is Boore and Atkinson (2008). The directivity pulse is the bump at about 3 seconds.

(>1Hz), the 3D velocity model has slightly lower spectral accelerations than the 1D model, particularly further from the fault into the soft basin, but for periods longer than 1 second (<1Hz), the 3D model has much higher spectral accelerations because of basin amplification. This is particularly strong around 17km from the fault where there is strong amplification at the northwestern edge of the Seattle basin. The directivity pulse at 0.3 seconds in the synthetic seismograms matches the period predicted by Shahi and Baker (2010). It also matches the amplitude quite well for the 1D model, but is exceeded by the 3D synthetics, suggesting that basin amplification effects are also found at these frequencies.

Site Amplification Transfer Functions

To validate the transfer functions that we computed for representative Vs profiles throughout Seattle using ProShake, we generated transfer functions for them using recordings of the Nisqually earthquake in 2001 as the input ground motions. We then compared the resulting transfer functions to the spectral ratios between accelerometers throughout the city and a soft rock site in Seward Park (SEW) as the reference site. These are shown on **Figure 10**. We did not expect to fit the exact peaks and troughs of amplification shown in the spectral ratios because representative profiles cannot replicate site specific peculiarities and because the spectral ratio is not a flawless representation of site response (e.g. Steidl et al., 1996). Instead we aim to roughly match the frequencies and amplitudes of amplification for most sites, and we achieve this with a few exceptions. The transfer functions match better than expected at some stations (e.g. WEK, THO, BRI, MAR), and quite well at less than 10Hz, but diverge at higher frequencies where shallow sublayers dominate the site response (e.g. TKCO, ALO, BHD, CRO, HOLY).

To validate the representative Vs profiles themselves, we compared the representative profiles for units where Vs profiles were actually measured by Wong et al., (2005) using Spectral Analysis of Surface Waves (SASW) for six sites dispersed throughout the city. We also compared the Vs30 values. (**Figure 11**). Again, we do not expect representative profiles to exactly match site-specific profiles, but they have very similar Vs30 values and the overall shape of several of the profiles is quite similar.

Seismically Induced Landslide Simulation using Nisqually Ground Motions

As mentioned earlier, only a few large earthquakes have hit the Seattle area since it's founding in the mid 1800's. All three were deep earthquakes with moderate ground motions and did not trigger extensive landsliding. As a result, we do not have any good seismically induced landslide distributions for the area to use to validate our methods. The 2001 M_w 6.8 Nisqually earthquake is the only of the three modern deep earthquakes for which dense ground acceleration records exist. It occurred during a rare dry period when it had not rained for a month (Stewart, 2005) so groundwater levels were low and very few landslides were triggered. As the best validation available, we ran the Nisqually ground motions through the seismically induced landslide simulation model using the factor of safety map for dry conditions to see if it reproduced what actually happened: i.e. few to no landslides triggered.

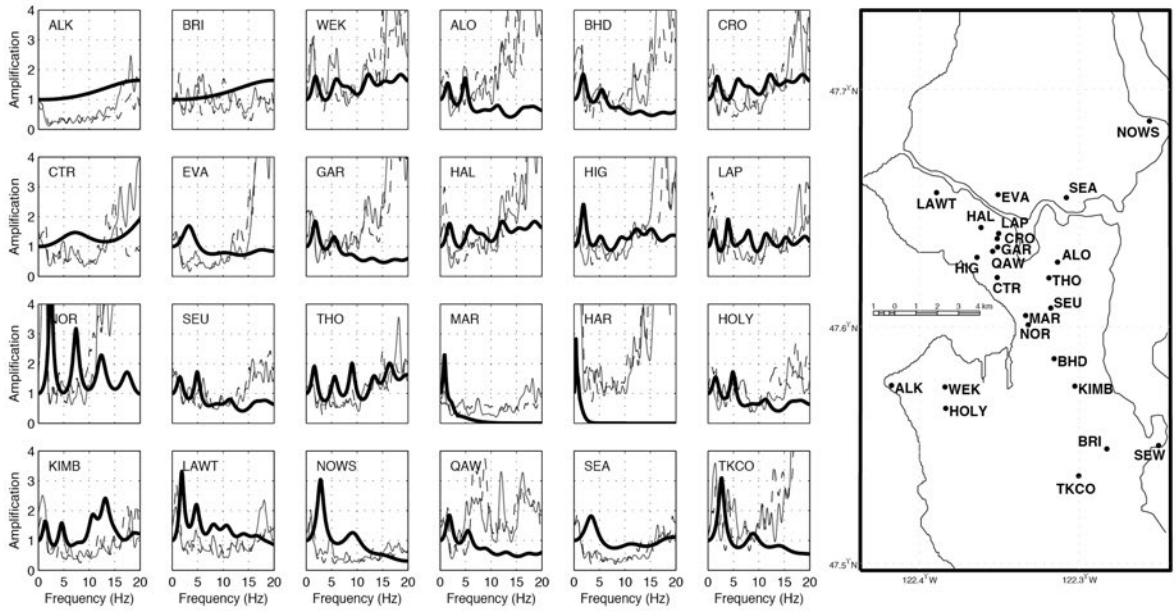

Figure 10 Comparison of transfer functions calculated for the representative Vs profiles that correspond to each station with the Nisqually ground motions using ProShake (thick black line) compared with the spectral ratio between each station and the soft-rock reference station, SEW, shown on the station map at right. North is dashed, East is solid.

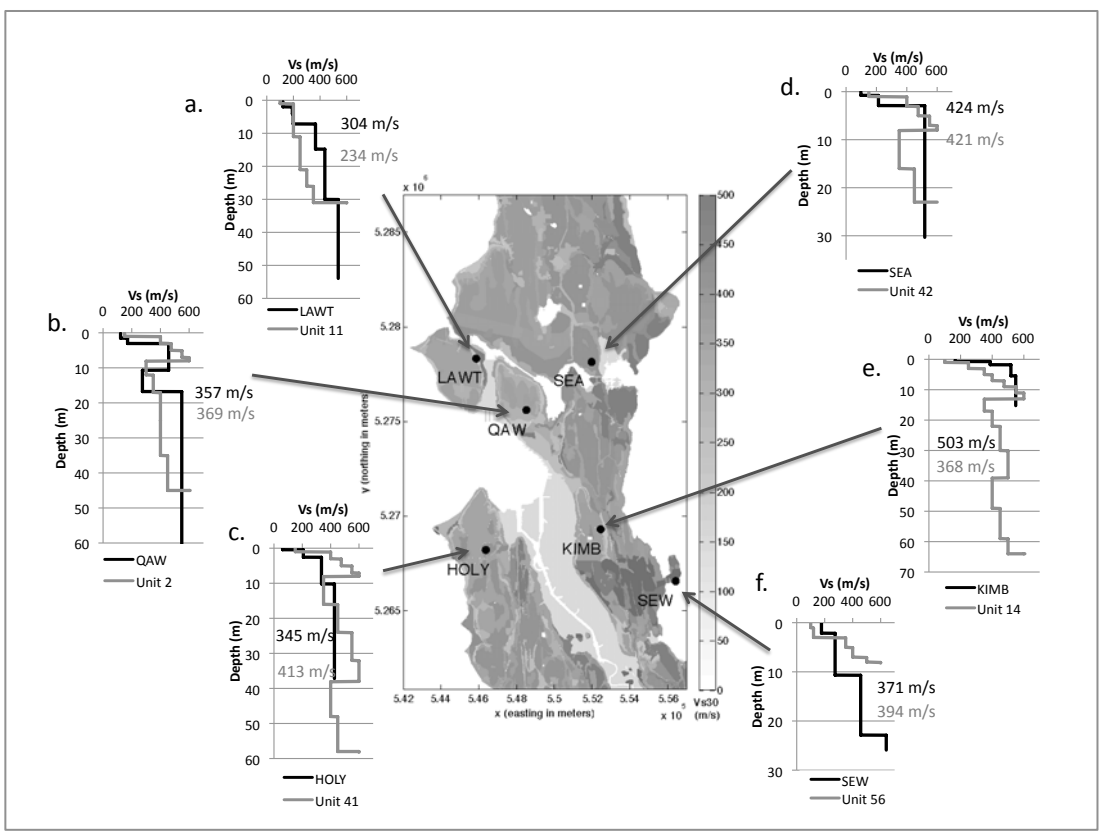

Figure 11 Vs profiles measured by Wong et al. (2011) at six seismic stations throughout Seattle (dark gray) compared to the representative Vs profiles we generated that correspond to the station locations (light gray). The Vs30 value that corresponds to each profile is marked next to the profiles. The background of the station map is the Vs30 map calculated from the representative profiles.

To do this, we used 33 strong ground motion records; the locations of 25 of these are shown on the map in Figure 10. In order to infer ground motion throughout the city from this sparse and irregular grid, we removed site amplification using spectral ratios relative to a reference site on a soft rock site in Seward Park (SEW). Then, the recording used for the seismically induced landslide simulation at each 210-meter grid point was the closest actual recording with the recording station's site effects removed, corrected for geometrical spreading and then readjusted for site effects using transfer functions developed for the representative Vs profiles we developed as input to ProShake using actual recordings of the Nisqually earthquake as the ground motion input. The ground motion during the Nisqually earthquake was more moderate than the Seattle fault simulation, so site amplifications are actually higher because they are not moderated by non-linear effects.

Table 2 Summary of Earthquake-Induced Landslide simulation results for Nisqually ground motions

	Dry Conditions[1]		Saturated Conditions[1]	
Number of failed 5x5m cells	31		14,478	
Number of sources[2]	21		7938	
Number of sources with >500m^2 area	0		13	
Maximum source size (m^2)	125		725	
Median slope of source cells (degrees)	42		35	
	Area (km^2)	%Land area[3]	Area (km^2)	%Land area
Sources	0.0008	0.0003%	0.36	0.16%
Sources and runout	0.0043	0.002%	1.53	0.67%
nmdisp[4] >0cm	0.028	0.01%	3.54	1.54%
nmdisp >5cm	0.0031	0.001%	1.09	0.48%
nmdisp >15cm	0.0017	0.0007%	0.74	0.32%
nmdisp >30cm	0.0010	0.0004%	0.51	0.22%

Notes:
1 Results using ground motions recorded during the 2001 M6.8 Nisqually earthquake adjusted for geometrical spreading and site amplification and interpolated using nearest neighbor on a 210m-grid throughout Seattle
2 Sources are clustered - adjacent "failed" cells are counted together as one source
3 Percent of total land area of Seattle. Seattle has a land area of ~229 km^2
4 nmdisp = Newmark Displacement

Table 2 summarizes the seismically-induced landslide simulation results for the Nisqually earthquake. The results for dry conditions - representative of the conditions during the Nisqually earthquake - predict 21 landslide sources, that, when combined with runout, covers an area of 4,300 m^2, less than the area of a football field. The locations of these slides are shown on **Figure 12**. They are located in seven localities around the city on bluffs with an average slope of 42°, steeper than the internal angle of friction for all Seattle geologic units (Harp et al., 2006). Only 0.0007% of the land area of Seattle had high landsliding potential (nmdisp>15cm). In reality, no large landslides were documented within Seattle city limits as triggered by the Nisqually earthquake because no comprehensive landslide survey was completed due to the lack of significant landsliding. However, it would be entirely possible for landsliding of the extent predicted by this model to go undocumented, particularly if it occurred in areas with no human impact such as parks or steep bluffs that are already

frequently struck by landslides. We consider this relative dearth of landsliding a validation that our earthquake-induced landslide simulation methods generate realistic results.

We also ran the landslide simulation with Nisqually ground motions for saturated soil conditions to see what might have happened if the Nisqually earthquake occurred at the same time as a high-intensity rainfall event. The results are drastically different. Nearly 8,000 landslide sources were generated, 13 of those greater than 500 m^2 in area. These sources and their runout cover 1.53 km^2 of the city, or about 300 football fields, and 0.3% of the land area of the city has high potential for landsliding (nmdisp>15cm).

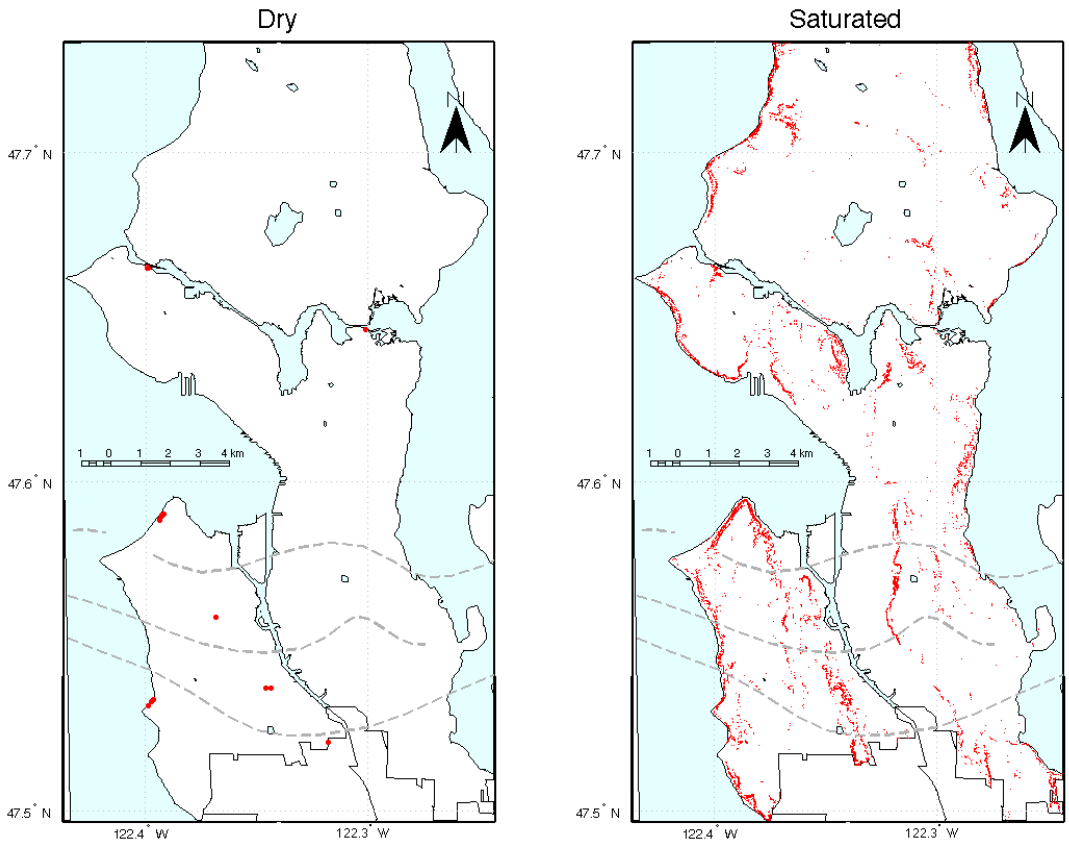

Figure 12 Landslide sources (red dots) triggered by the simulation for dry (left) and saturated (right) conditions using ground motions from the 2001 Mw6.8 Nisqually earthquake. Marker sizes are larger than the cell size in order to be visible on this map scale.

Results of Mw 7 Seattle Fault Earthquake Simulation

Table 3 summarizes the results of our seismically induced landslide simulation for the scenario M_w 7 Seattle fault earthquake for the best- and worst-case scenarios, corresponding to dry and saturated soil conditions respectively. The location of landslide sources for both scenarios is shown on **Figure 13**. These results were calculated using the broadband seismograms generated with a 3D velocity model of the Seattle basin and then adjusted for 1D site amplification and an approximation of topographic amplification as described in the methods section. We also present maps showing relative seismically induced landslide hazard for a M_w 7 Seattle fault earthquake (**Maps 1 and 2**). Hazard levels are based on Newmark displacement where 0-5cm is considered low hazard, 5-15cm is moderate, 15-30cm is high

and >30cm is extremely high. Note that there are some areas that show up as high or extremely high landslide hazard that are actually manmade structures that were not completely removed from the LIDAR imagery used to obtain slope angles, for example the Husky Stadium and rock and cement retaining walls around houses in hilly neighborhoods. This must be taken into consideration when looking in detail at certain areas of the city.

Dry Soil Conditions

The results of the simulation for dry soil conditions, meaning the soil is not saturated in the top few meters, is the most realistic scenario and these are the results we will focus on. The simulation generates 6,535 landslide sources covering 0.32 km^2. Landslide sources and their runout together cover about 1 km^2, less than half a percent of the city's land area. 14 landslide sources are larger than 500 m^2 and 0.17% of the city is in a high seismically induced landslide hazard zone (nmdisp>15cm). Landsliding is concentrated in the southern half of the city along the coastal bluffs of West Seattle, the western side of Beacon Hill along I-5 and scattered throughout Delridge. The coastal bluffs of Magnolia and Queen Anne show less concentrated landsliding, and North Seattle escapes relatively unharmed with the exception of localized landsliding along coastal bluffs in North Ballard, near Carkeek Park, and in Lake City (Figure 13, left).

Table 3 Summary of Earthquake-induced Landslide Simulation results for Mw 7 Seattle Fault Earthquake Scenario

	Dry Conditions[1]		Saturated Conditions[1]	
seismogram->	**unfiltered**		**unfiltered**	
Number of failed 5x5m cells	12,794		100,060	
Number of sources[2]	6535		41816	
Number of sources with >500m^2 area	14		339	
Maximum source size (m^2)	1,550		3,375	
Median slope of source cells (degrees)	27		23	
	Area (km^2)	%Land area[3]	Area (km^2)	%Land area[3]
Sources	0.32	0.14%	2.50	1.09%
Sources and runout	1.11	0.48%	7.06	3.08%
nmdisp[4] >0cm	3.49	1.50%	14.43	6.29%
nmdisp >5cm	0.98	0.43%	7.99	3.48%
nmdisp >15cm	0.39	0.17%	5.46	2.38%
nmdisp >30cm	0.16	0.07%	3.78	1.65%

Notes:
1 Results using broadband synthetic seismograms generated using a 3D velocity model and including site amplification
2 Sources are clustered - adjacent "failed" cells are counted together as one source
3 Percent of total land area of Seattle. Seattle has a land area of ~229 km^2
4 nmdisp = Newmark Displacement

Saturated Soil Conditions

When we run the same exact scenario with the factor of safety map for saturated conditions, the results are much more drastic. Over 40,000 landslides are generated, with sources and runout covering 7km^2, equal to 3% of the land area of the city. There are over 300 landslides with an area of more than 500 m^2. 2.4% of the city is now in a high landslide hazard zone

(nmdisp>15cm). Fortunately this scenario represents a highly unlikely event of an earthquake striking when the water table is effectively at the surface from higher than normal rainfall topped with a severe precipitation event.

The distribution of landslide sources for saturated conditions contrasts with the dry scenario (**Figure 13**). The southern half of Seattle is devastated, dense landsliding is concentrated not only on the typical coastal bluffs and along the Duwamish valley, but also scattered throughout West Seattle, Delridge, Beacon Hill, Seward Park and Rainier Valley. Landsliding rims both Magnolia and Queen Anne and extends north along I-5 all the way to Portage bay. North Seattle, though less hard-hit than the rest of the city, is more severely affected in the saturated scenario. The coastal bluffs along Puget Sound experience dense landsliding in incised valleys up to a kilometer back from the coast, particularly in the northwest corner of the city because of the strong amplification of low frequencies at the edge of the basin.

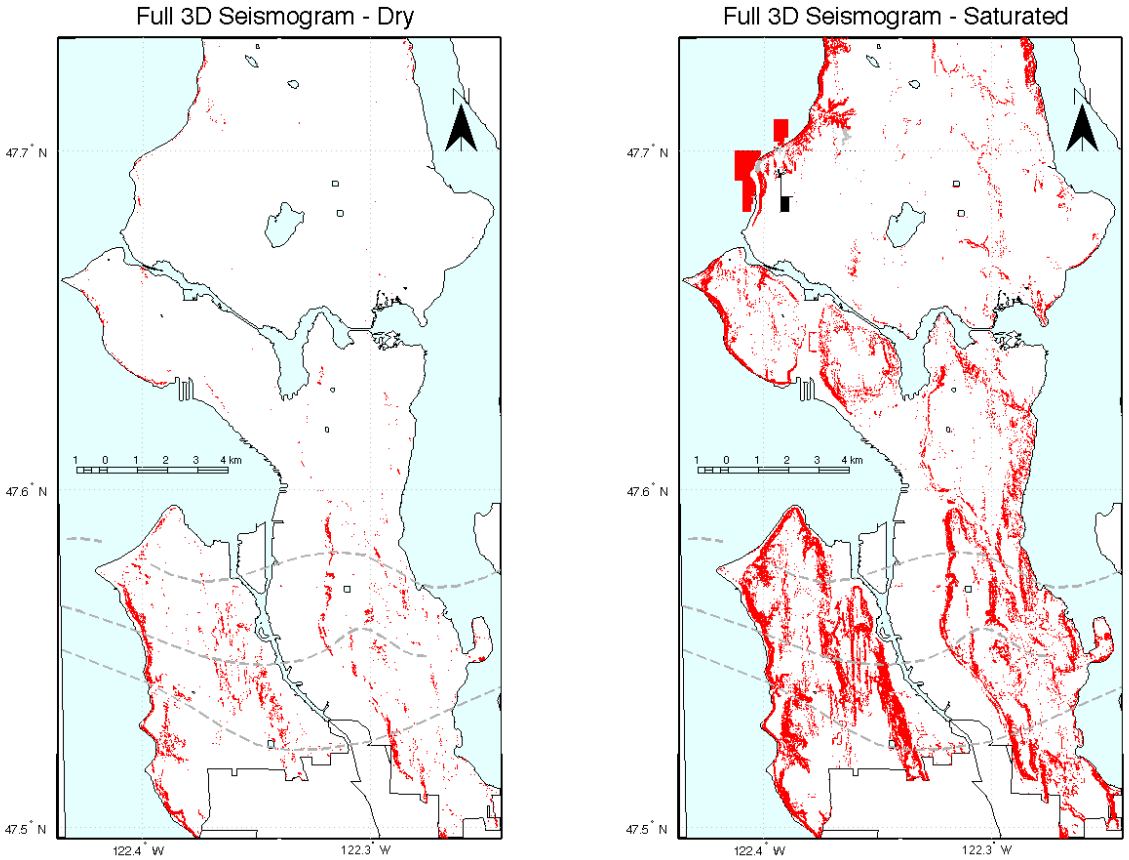

Figure 13 Landslide sources (red) triggered by the simulation for dry (left) and saturated (right) using the broadband synthetic seismograms generated for a Seattle Fault earthquake using a 3D basin velocity model. The markers are larger than the area of the cell they represent ($25m^2$) in order to be visible so the total area affected by landslide appears larger than it is.

Discussion

Particularly Vulnerable Areas and Infrastructure

Areas of steep topography on the hanging wall of the Seattle fault are most severely affected by seismically induced landsliding. It is not only the coastal bluffs, but landsliding also extends to inland slopes and threatens many key transit routes and buildings. North and east of downtown, though hard hit in the less likely saturated scenario, are actually not that bad in the more realistic dry scenario, though there are some localized areas of concern.

Zoom-ins representing some areas of concern are shown on **Figure 14** that shows landslide sources and runout for dry soil conditions. Railroad tracks running along the base of the steep coastal bluffs of North Seattle may be blocked by landslide runout (**Figure 14A**). Houses built above and below the steep bluffs along Lake Washington in Lake City may be at risk (**Figure 14B**). Steep slopes that run along the east side of I-5 south of downtown are highly susceptible to seismically induced landslides. Some runout from these slides crosses I-5 in this scenario, but our model does not take into account elevated areas of highway nor does it adjust for areas that are already mitigated for landsliding, so the landslide runout intersections with I-5 may be overestimated. Large deep-seated landslides may be the greatest threat to this key transit corridor, based on the landslide scars that stand out in the LIDAR imagery (**Figure 14C**). Several key access roads to West Seattle, such as the one shown on **Figure 14D**, could be blocked by landslide runout according to this simulation and would need to be cleared quickly for rescuers to reach West Seattle. The steep areas along Puget Sound at the western edge of West Seattle is probably the most at-risk area overall. **Figure 14E** is just one of many examples of concentrated landsliding sources and runout intersecting numerous private homes built along and below the steep bluffs. **Figure 14F** demonstrates that access to ferry to Vashon Island may be blocked by landslides and their runout as well.

We quantified the intersection of triggered landslide sources and runout with infrastructure maps available from the City of Seattle GIS database. We looked at building outlines, water, sewer and electric lines, and transit. These results are summarized on **Table 4**. The numbers we present are a very rough calculation of the extent of each type of infrastructure that might be impacted. Also, as mentioned earlier, runout distances may be overestimated for the dry scenario. The simulation is probabilistic so we do not claim that the exact features intersected in this scenario will be hit by landslides in real life, nor do we claim that if they are impacted, they will necessarily be damaged beyond use, just that our simulation shows the landslides and infrastructure intersect. *So these numbers should not be taken as an exact representation of what will happen, but instead as an order of magnitude estimate of the extent of damage we should expect.* **Figure 15** shows a citywide plot of the point locations of where intersected infrastructure is located, highlighting areas that should expect high infrastructure impacts. Note that some infrastructure, such as buried water and sewer lines and elevated electric lines, may be more susceptible to damage by landslides sources and may be unaffected by runout.

We also calculated intersections with key public buildings such as hospitals, schools, emergency operations centers and police and fire stations, and found none of these buildings were intersected by landslides or runout for both dry and saturated conditions. However, the

GIS layers available to use only showed the locations of these buildings as point locations instead of building outlines, so they need to be reanalyzed if building outlines for these public buildings become available to be sure they are not threatened.

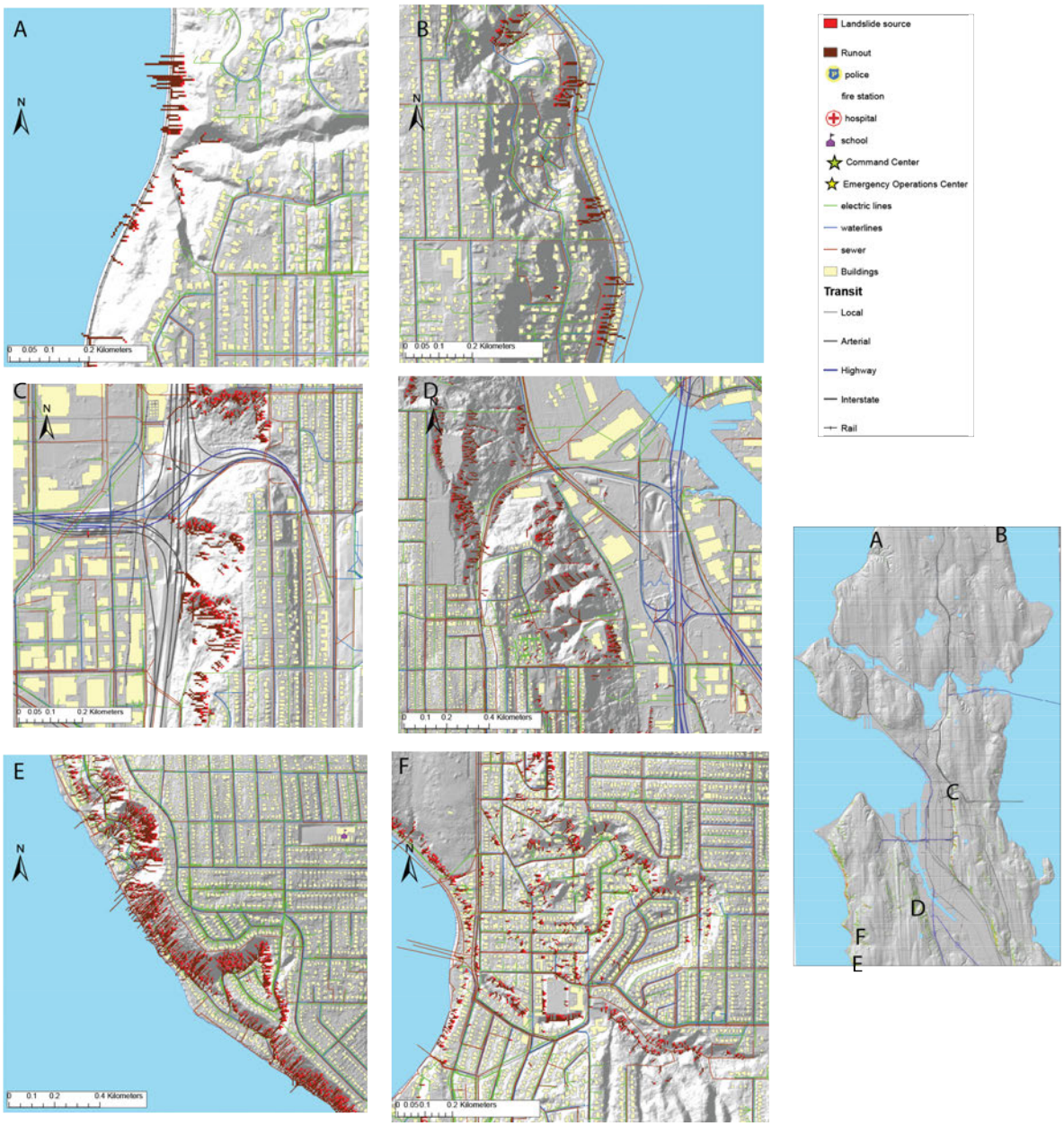

Figure 14 Zoom-ins on a few areas of concern showing landslide sources (red) and runout (brown) as well as infrastructure and building outlines. Locations of each zoom-in are shown on map of Seattle at right. See text for detailed descriptions.

Table 4 Intersections between triggered landslides and infrastructure

	Dry conditions		Saturated conditions	
	source	runout	source	runout
Number of buildings	317	963	2134	5437
Water lines (km)	0.75	5.45	5.8	37.6
Sewer lines (km)	1.3	7.7	12.4	60.7
Electric lines (km)	1.6	6.1	18.4	49.8
Transit				
local (km)	0.6	3.5	5.1	33.9
arterial (km)	0.005	0.7	0.6	7.6
highway (km)	0.002	0.006	0.1	0.3
interstate (km)	0.001	0.5	0.5	2.4
rail (km)	0.004	0.4	0.2	2.2

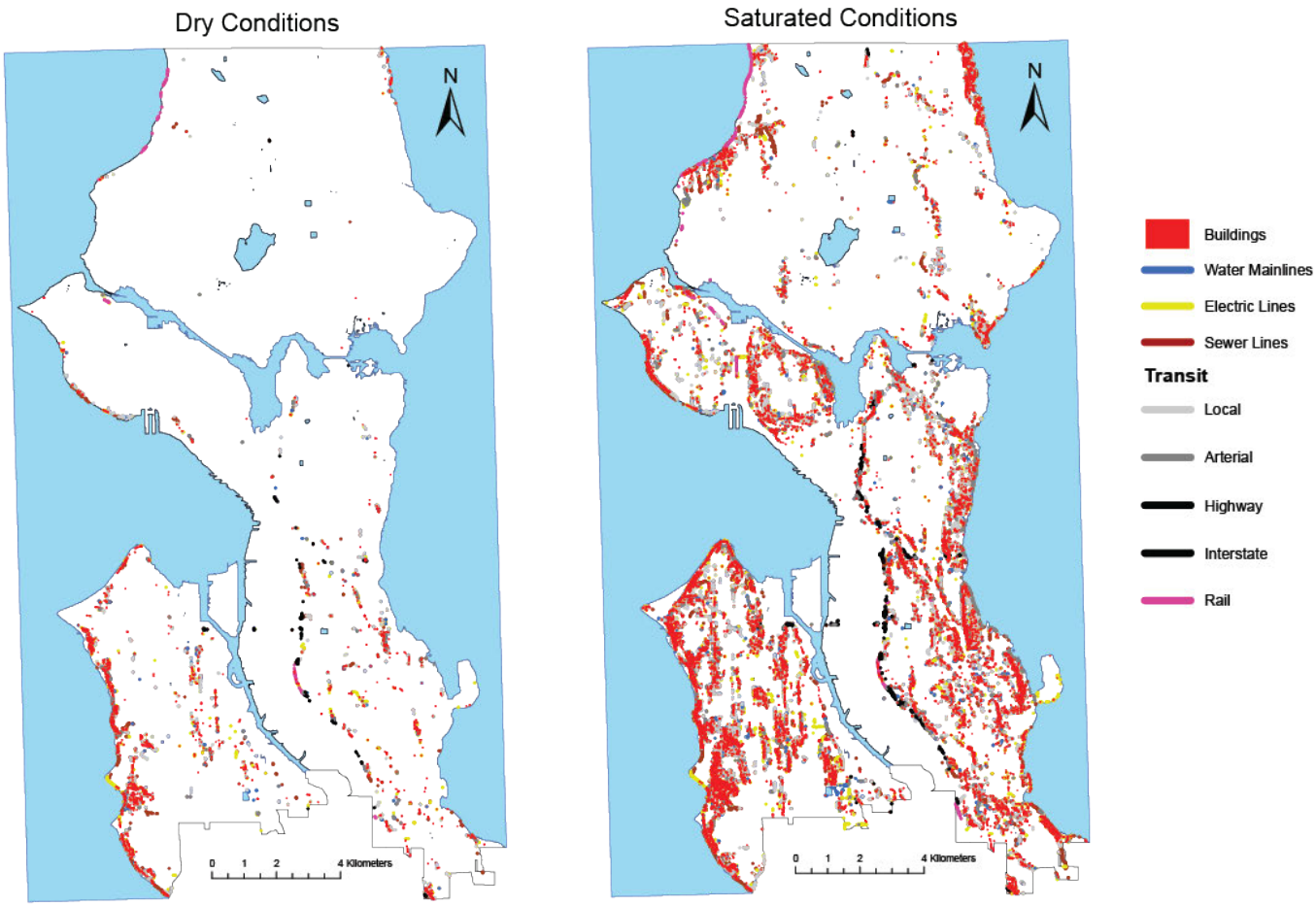

Figure 15 Map showing the citywide distribution of point sources of infrastructure intersected by landslide sources and runout.

Comparison with Previously Designated Landslide-prone Areas

While overall patterns of landsliding correspond to areas that are generally known to be landslide prone, a surprising percentage of the landslides triggered by the seismically induced

landsliding simulation are in areas of low and medium relative hazard for landsliding based on static slope stability as delineated by Harp et al. (2006). **Table 5** summarizes this comparison. About 9% of the total landslides triggered by our simulation occur in low landslide hazard areas for dry conditions, and 13% for the saturated scenario. These of course represent a tiny fraction of the citywide area designated as low hazard (0.02% and 0.2% respectively), but demonstrate that we cannot assume that seismically induced landslides will only be triggered in areas already designated as hazardous by studies focusing on static slope stability where water is the primary natural trigger.

Similarly, a comparison between the cells that failed in the seismically induced landslide simulation and areas designated as 'potential sliding areas' in the City of Seattle corporate GIS database (©City of Seattle) also shows that a significant percentage of the triggered landsides lay outside the designated areas. For dry conditions, 42% of failed cells are outside potential sliding areas, 45% for saturated conditions. The potential sliding areas were designated based on the contact between a permeable and impermeable geologic unit (Esperance sand and Lawton clay) where seepage occurs and many historical landslides have been triggered by water and are not necessarily inclusive of areas prone to landsliding triggered by ground motion.

Table 5 Comparison of seismically induced landslides triggered by a Mw7 Seattle fault earthquake and relative static landslide hazard designations

	Dry conditions			Saturated Conditions		
Relative Landslide Hazard[1]	**Number of failed 5x5m cells**	**% of total failed cells**	**% of total cells with same hazard level**	**Number of failed 5x5m cells**	**% of total failed cells**	**% of total cells with same hazard level**
High (FS[2]<1.5)	7986	62%	4%	48022	48%	25%
Medium (2.5>FS>1.5)	3691	29%	1%	39371	39%	10%
Low (FS>2.5)	1106	9%	0.02%	12667	13%	0.2%

1) as reported in Harp et al., (2006)
2) Factor of Safety

Importance of Various Levels of Complexity

In the previous section we presented results generated using synthetic ground motions calculated at a high level of complexity: broadband frequency content in the ground motions, 3D basin amplification and 1D soil amplification - but the inclusion of this complexity was time consuming. In order to determine what parts of the effort were worthwhile, and what parts could be neglected in future work without significantly altering the results, we look at the importance of different levels of complexity on the results.

Figure 16 compares the effect of the levels of complexity on the total number of failed 5x5m cells for dry and saturated conditions that will be discussed in the following sections.

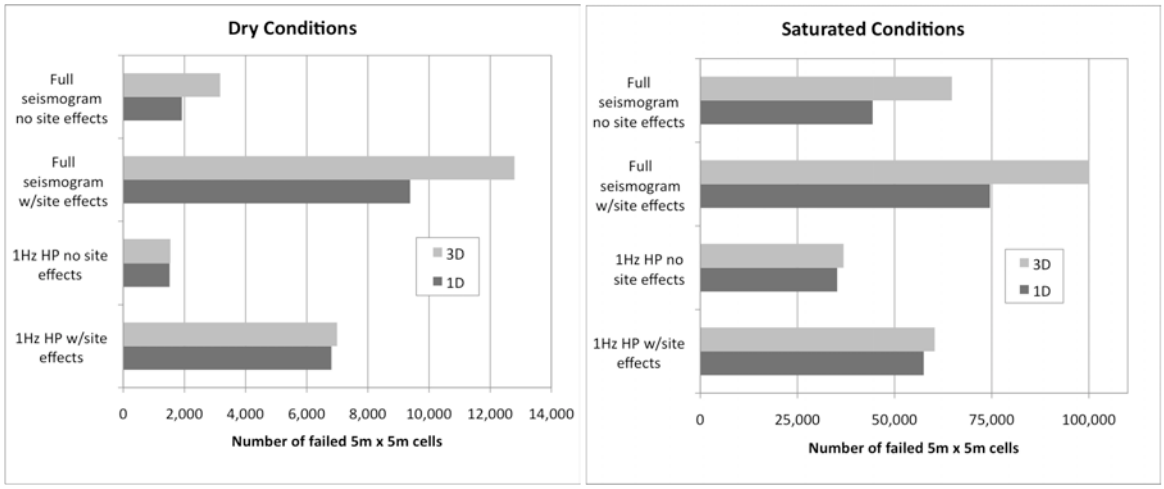

Figure 16 Comparison of the number of failed cells triggered by the M7 Seattle fault earthquake simulation for different levels of complexity: 3D=using synthetics generated using 3D velocity model, 1D=using synthetics generated using a 1D velocity model, Full Seismogram= using unfiltered broadband synthetic seismograms, 1Hz HP=using synthetics highpass filtered with a corner frequency of 1Hz, site effects=results calculated using transfer functions generated in ProShake for representative Vs profiles to approximate 1D site amplification.

Site amplification

The inclusion of 1D site amplification is the most important level of complexity. It has an enormous influence on the outcome. For dry conditions, including site amplification in the simulation more than quadruples the number of failed cells for dry conditions, even though the transfer functions account for non-linear effects that decrease motion in many areas of the city. For wet conditions the effect is much smaller, probably because the probability of failure curve levels out at 34% at about 17cm displacement (see Figure 3). When displacements are already high, as they are for wet conditions, site effects make them higher, but don't significantly increase the probability of failure so the number of failures does not greatly increase. *This shows that 1D site amplification needs to be included, and ignoring it could result in a severe underprediction of seismically induced landsliding.*

Basin Amplification (3D velocity model)

As mentioned earlier, 3D amplification in the sedimentary basin underlying the north part of Seattle is accounted for in the simulations by using a 3D basin model to generate the synthetic seismograms. The importance of adding this extra level of complexity rather than just using a simpler 1D velocity model is highlighted on **Figure 16**. The inclusion of basin amplification bumps up the number of slope failures by about 30% when the full seismogram is used. If we use the 1Hz highpass filtered seismograms, there is very little difference in the results because the basin amplification effects are all below 1Hz and are filtered out. *In an area that does not sit on a significant sedimentary basin, the 1D velocity model would be sufficient, but for Seattle, which does site upon a basin, using a 3D basin model is critical.*

Frequency Content

The results presented in the previous section were calculated without accounting for any frequency dependence of seismically induced landslides. The Newmark method is independent of frequency and just depends on the absolute slope-parallel acceleration. It does end up having some frequency dependence because long period waves have wider pulses and can exceed the critical acceleration for a longer time and contribute much more displacement

than a high frequency pulse that reaches the same maximum amplitude. However, this is moderated because longer period motion is typically lower in amplitude and will not exceed the critical acceleration on its own, but can be important because it boosts higher frequency pulses higher above the critical acceleration so more displacement can accumulate.

However, field observations of landslide distributions after earthquakes suggest that there may be frequency dependence beyond that simple scenario and that landslides triggered by earthquakes may be most sensitive to frequencies between 1 and 10Hz (Jibson et al., 2004). Whether this is due to site-specific amplifications in pre-weakened slopes (e.g. Allstadt et al., 2009, Moore et al., 2011), another mechanism such as the wavelength of motion and coherence of ground displacement, or simply due to the fact that ground accelerations are typically higher in this frequency range, is a topic that demands more research.

If we run the landslide simulation using all the exact same methods, but highpass filter the synthetic seismograms above 1Hz to exclude the influence of longer period motion, we nearly cut the total number of failed cells in half for both dry and saturated conditions (Figure 16). The distribution of landsliding is similar in both cases but the Newmark displacements are lower when we filter out the lower frequencies and therefore fewer cells fail.

However, this 1 Hz lower limit for triggering shallow landslides is based on expert opinion and is not agreed on by all experts. There is no particular reason we couldn't instead filter at 0.3Hz or 2Hz and use those results. If we quantify the contribution of each frequency to generating Newmark displacement we see that the selection of an arbitrary frequency cutoff makes a huge difference to the total Newmark displacement (**Figure 17**). In order to do this, we cannot simply run the landslide simulation with seismograms bandpass filtered because that would downplay the importance of the lower frequencies because they primarily act as a booster for the higher frequency energy. Instead we progressively highpass filter the long periods out, while allowing higher frequencies to remain to see how important the long periods are.

Figure 17 shows the ratio of Newmark displacement at each highpass to the total Newmark displacement obtained without any filtering. This shows that for the 3D simulation, only about 45% of the total Newmark displacement is accumulated citywide if the seismograms are highpass filtered with a corner frequency of 1Hz and it falls off steeply when highpassed above that. If we choose 0.3Hz instead, we get 80% of the total displacement, if we choose 2Hz, we get 30% of the displacement. Slight variations in this somewhat arbitrary frequency cutoff result in significant differences in the Newmark displacement. The effect is less severe for the 1D simulation, 70% of the total Newmark displacement is reached with the 1Hz highpass, 90-100% if we use 0.3Hz, but the total Newmark displacement drops off faster at higher frequencies.

The extreme sensitivity to this semi-arbitrary frequency cutoff makes it is clear that the frequency dependence of triggered landsliding needs to be researched. Until the sensitivity relationship between landslide size and frequency of ground motion can be quantified, and it can be clearly demonstrated that shallow landslides are not sensitive to lower frequency ground motion, we have decided to use the unfiltered broadband seismograms for the final results.

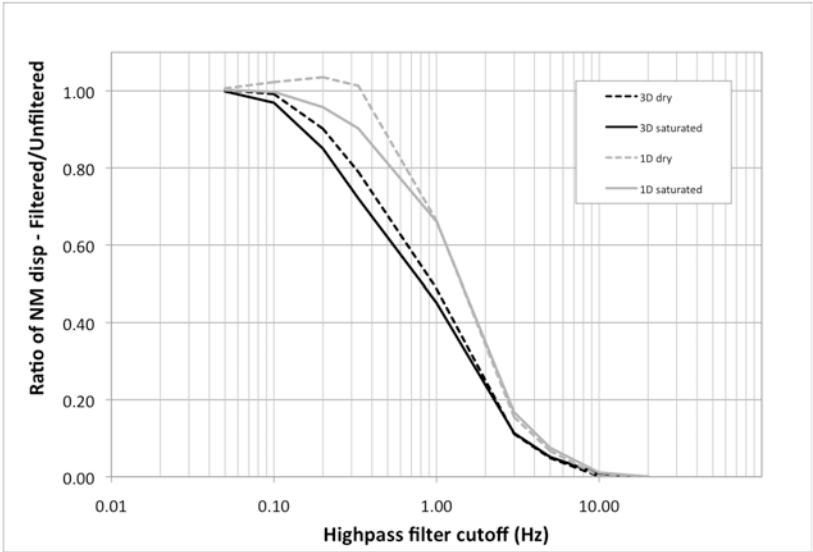

Figure 17 The importance of each frequency to the accumulation of Newmark displacement. The plot shows the ratio of total city-wide Newmark displacement generated when the synthetic seismograms are highpass filtered at a range of corner frequencies to the total Newmark displacement generated by the full unfiltered seismograms. Results are shown for Saturated (black) and Dry (gray) conditions for synthetics generated using both a 1D (dashed) and a 3D (solid) velocity model. Site amplification is included in all results. The synthetic seismograms generated using a 3D velocity model that include basin amplification effects at low frequencies generate less than half the Newmark displacement when frequencies below 1Hz are filtered out. The effect is not as strong for the 1D synthetics that do not have basin amplification at long periods, 70% of the total Newmark displacement is still generated if frequencies below 1Hz are filtered out.

Conclusions

The results of this study show that seismically induced landsliding would significantly impact Seattle's residents and its infrastructure if a large earthquake were to occur on the Seattle Fault. The southern half of the city located on the hanging wall of the fault will be particularly hard hit, while north Seattle is the least impacted with the exception of localized areas particularly along coastal bluffs. Several hundred to thousand buildings could be affected citywide; many kilometers of roads could be obstructed, including some key transit routes such as I-5 and access roads to West Seattle. If the groundwater table is low when the earthquake hits, as simulated by the dry scenario, the total area of landslide sources will be nearly an order of magnitude smaller than if the subsurface is completely saturated.

Future Work

The high impact of landsliding predicted by this seismically induced landsliding simulation for a Seattle Fault earthquake shows that this secondary effect of earthquakes should be studied with as much vigor as other earthquake effects.

Logical next steps include looking at the stability of these results for other randomized rupture models of a large Seattle earthquake and also running the simulation for different potential earthquakes, including some more moderate earthquakes on the Seattle fault and on nearby crustal faults, deep Benioff zone earthquakes of a range of magnitudes, and megathrust Cascadia subduction events.

In addition, there is a vast difference between the extent of landsliding triggered for dry conditions and saturated conditions, representing a minimum and maximum extent of

landsliding. We only computed these two extremes because those are the conditions for which preexisting factor of safety maps have been made, but a simulation that includes a range of levels of ground saturation could make the results more realistic. This would require recalculating the factor of safety for Seattle for a range of saturation thicknesses.

We also did not investigate deep-seated block landsliding, which was a problem during past earthquakes in Seattle, as evidenced by the remains of entire blocks of forest in the bottom of Lake Washington (Karlin and Abella, 1992). This is something that should be investigated because of the vast potential impacts of just one deep-seated landslide in the now densely populated city.

Furthermore, this method of using synthetic seismograms as input for a regional Newmark analysis has not been done before, and though we validated it with ground motions for the 2001 Mw 6.8 Nisqually earthquake that did not trigger much landsliding in Seattle, a better validation could be done by generating synthetic seismograms for an earthquake that already occurred that triggered extensive landsliding, has dense ground motion recordings for validation of the synthetic seismograms, and for which a complete triggered landslide survey was completed. One possibility is the 1997 Northridge earthquake.

There are some parts of the methodology that could use some improvements to be more accurate for Seattle's geology including modifying the curve that relates Newmark displacement probability of landsliding curve to better represent the behavior of the moist unconsolidated soils found throughout much of Seattle. The runout estimation methods could be improved to avoid overestimating impacts for landslides triggered in dry soil conditions, and the representative Vs profiles representative of Seattle's geology could use more refinement.

Finally, there is the question of the frequency dependence of seismically induced landsliding addressed in the discussion section. This is a topic that requires more investigation because we found in this work that if we filter out the lower frequency (<1Hz) portion of the signal that some argue shallow landslides are not sensitive to, we significantly decrease the total number of landslides triggered and eliminate the contribution of directivity pulses and basin amplification to landslide triggering. At present, it is unclear whether frequency dependence or frequency independence of shallow landsliding is more representative of reality, but answering this question is critical to defining seismically induced landslide hazard in Seattle, where basin amplification at low frequencies can be strong.

Acknowledgements

Many thanks to Randy Jibson, Art Frankel, Steve Kramer, Ed Harp, Andy Delorey, Kathy Troost, John Michael, Tim Walsh, Isabelle Sarikhan, and the City of Seattle, for sharing data, ideas, and advice.

References

Aki, K. and Larner, K.L., 1970, Surface motion of a layered medium having an irregular interface due to incident plane SH waves, J.Geophys.Res, v.75, p933-954.

Allstadt, K., 2009, Study of Site Effects in Landslides using Weak Ground Motion, Avignonet and Séchilienne Landslides, French Alps, M.S. Thesis, Université Joseph Fourier and ROSE School. 87p.

Ashford, S.A., Sitar, N., Lysmer, J., and Deng, N., 1997, Topographic Effects on the Seismic Response of Steep Slopes: Bull. of Seis. Soc. of Am., v.87, p701-709.

Bard, P-Y., and Tucker, B.E., 1985, Underground and Ridge Site Effects: A Comparision of Observation and Theory: Bull. of Seis. Soc. of Am., v75, p.905- 922.

Blakely, R.J., Wells, R.E., Weaver, C.S., and Johnson, S.Y., 2002, Location, structure, and seismicity of the Seattle fault zone, Washington: evidence from aeromagnetic anomalies, geologic mapping, and seismic-reflection data. Geological Society of America Bulletin, 114, p. 169-177.

Boore, D.M., 1972, Note on the effect of simple topography on seismic SH waves: Bull. Seis. Soc. of Am., v.62, p275-284.

Boore, D.M., 1983, Stochastic simulation of high-frequency ground motions based on seismological models of the radiated spectra: BSSA., v.73, p.1865-1894.

Boore, D.M., 1996, SMSIM-Fortran programs for simulating ground motions from earthquakes: version 1.0, U.S. Geol.Surv. Open-File Rept. 96-80-A, 73p.

Boore, D.M. and Atkinson, G.M., 2008, Ground-motion prediction equations for the average horizontal component of PGA, PGV and 5%—damped PSA at spectral periods between 0.01 s and 10.0 s. Earthquake Spectra, EERI 24 (1), 99–138.

Bucknam, R.C., Hemphill-Haley, E. and Leopold, E.B., 1992, Abrupt Uplift Within the Past 1700 Years at Southern Puget Sound, Washington: Science, v.258, p.1611-1614.

Campbell, K.W. and Borzorgnia, Y., 2008, NGA ground motion model for the geometric mean horizontal component of PGA, PGV, PGD and 5% damped linear elastic response spectra for periods ranging from 0.01 to 10 s, Earthq.Spectra 24, 139-172.

Chiou, B.S.J., and Youngs, R.R., 2008, Chiou-Youngs NGA ground motion relations for the geometric mean horizontal component of peak and spectral ground motion parameters, Earthquake Spectra 24, 173-216

Chleborad, A.F. and Schuster, R.L., 1998, Ground failure associated with the Puget Sound region earthquakes of April 13, 1949, and April 29, 1965. USGS Professional Paper, P 1560, pp 373–439.

Choi, Y. and Stewart, J.P., 2002, Nonlinear site amplification as a function of 30m shear wave velocity: Earthquake Spectra, v.21, p.1-30.

Coe, J.A., Michael, J.A., Crovelli, R.A., Savage, W.Z., Laprade, W.T. and Nashem, W.D., 2004, Probabilistic assessment of precipitation-triggered landslides using historical records of landslides occurrence, Seattle, Washington. Environmental & Engineering Geoscience, v.2, p103-112.

Delorey, A.A. and J.E. Vidale, 2010, Seattle Basin shear-velocity model from noise correlation Rayleigh waves, Seism. Res. Lett., v.81, p.305.

Frankel, A.D., Carver, D.L., and Williams, R.A., 2002, Nonlinear and Linear Site Response and Basin Effects in Seattle for the M6.8 Nisqually, Washington, Earthquake: Bull. of Seis. Soc. of Am., v.92, p.2090-2109.

Frankel, A.D., Stephenson, W.J., Carver, D.L., Williams, R.A., Odum, J.K., and Rhea, S., 2007, Seismic hazard maps for Seattle incorporating 3D sedimentary basin effects, nonlinear site response, and rupture directivity, U.S. Geol. Surv. Open-File Rept. 07-1175, 70 pp.

Frankel, A.D., 2009, A Constant Stress-Drop Model for Producing Broadband Synthetic Seismograms: Comparison with the Next Generation Attenuation Relations: Bull of Seis Soc of Am., v.99, p664-680.

Geli, L., Bard, P.-Y., Jullien, B., 1988, The effect of topography on earthquake ground motion: a review and new results: Bull. of the Seis. Soc. of Am., v.78, p.42– 63.

Godt, J., Sener,B., Verdin,K., Wald,D., Earle,P., Harp,E., and Jibson,R., 2008, Rapid assessment of earthquake-induced landsliding, Proceedings of the First World Landslide Forum, United Nations University, Tokyo, Japan, 4 p.

Harp, E.L., and Jibson, R.W., 2002, Anomalous Concentrations of Seismically Triggered Rock Falls In Pacoima Canyon: Are They Caused by Highly Susceptible Slopes or Local Amplification of Seismic Shaking?, Bull. of Seis. Soc. of Am., v.92, p3180-3189.

Harp, E.L., Michael, J.A., and Laprade, W.T., 2006, Shallow-Landslide Hazard Map of Seattle, Washington, USGS Open-File Report 2006-1139, 23p.

Hartzell, S., Carver, D., Cranswick, E. and Frankel, A., 2000, Variability of Site Response in Seattle, Washington: Bull. of Seis. Soc. of Am., v.90, p.1237-1250.

Highland, L.M., 2003, An Account of Preliminary Landslide Damage and Losses Resulting from the February 28, 2001, Nisqually, Washington, Earthquake: USGS Open-File Report 03-211, 48p.

Hopper, M.G., 1981, A study of liquefaction and other types of earthquake-induced ground failures in the Puget Sound, Washington, region: Blacksburg, Va., Virginia Polytechnic and State University M.S. thesis, 131 p.

Hunter, G. and Fell, R., 2003, Travel distance angle for "rapid" landslides in constructed and natural slopes: Canadian Geotech J., v.40, p.1123-1141.

Jacoby, G.C., Williams, P.L. and Buckley, B.M., 1992, Tree Ring Correlation Between Prehistoric Landslides and Abrupt Tectonic Events in Seattle, Washington: Science, v.258, p.1621-1623.

Jibson, R.W., Harp, E.L., and Michael, J.A., 2000, A method for producing digital probabilistic seismic landslide hazard maps: Engineering Geology, v.58, p.271-289.

Jibson, R.W., Harp, E.L., Schulz, W., Keefer, D.K., 2004. Landslides triggered by the 2002 M-7.9 Denali Fault, Alaska, earthquake and the inferred nature of the strong shaking. Earthquake Spectra 20, 669–691.

Jibson, R.W., 2007, Regression Models for estimating coseismic displacement: Engineering Geology, v.91, 209-218.

Jibson, R.W. and Michael, J.A., 2009, Maps Showing Seismic Landslide Hazards in Anchorage, Alaska: Pamphlet to accompany USGS Scientific Investigations Map 3077.

Johnson, S.Y., Dadisman, S.V., Childs, J.R. and Stanley, W.D., 1999, Active tectonics of the Seattle fault and central Puget Sound, Washington – Implications for earthquake hazards: Geol. Soc. of Am. Bull., v.111, p1042-1053.

Karlin, R.E. and Abella, S.E.B., 1992, Paleoearthquakes in the Puget Sound Region Recorded Sediments from Lake Washington, USA: Science, v.258, p.1617-1620.

Karlin, R.E., Holmes, M., Abella, S.E.B., and Sylvester, R., 2004, Holocene landslides and a 3500-year record of Pacific Northwest earthquakes from sediments in Lake Washington: GSA Bull., v.116, p94-108.

Keefer, D.K., 1983, Landslides, soil liquefaction, and related ground failures in Puget Sound earthquakes, in Yount, J.C., and Crosson, R.S., eds., Proceedings of Workshop XIV, Earthquake hazards of the Puget Sound region, Washington, October 13–15, 1980, Lake Wilderness, Wash.: U.S. Geological Survey Open-File Report 83–19, p. 280–299.

Keefer, D., 1984, Landslides caused by earthquakes: Geol. Soc. of Amer., v.95, p.406-421.

Keefer, D., 2002, Investigating Landslides Caused by Earthquakes – A Historical Review: Surveys in Geophysics, v23., 473-510.

Laprade, W.T., Kirkland, T.E., Nashem, W.D., Robertson, C.A., 2000, Seattle landslide study. Shannon and Wilson, Inc. Internal Report W-7992-01.

Liu, P. C., and Archuleta,R.J., 2002, The effect of a low-velocity surface layer on simulated ground motion, Seismol. Res. Lett 73, 267.

Logan, R. L., Pringle, P. T., Schuster, R. L., 1998, Timing of large and possibly seismically induced landslides on the Olympic Peninsula and Lake Sammamish, Washington [abstract]: Association of Engineering Geologists, 41st Annual Meeting, Program with Abstracts, p. 107.

Ludwin, R.S., Thrush, C.P., James, K., Buerge, D., Jonientz-Trisler, C., Rasmussen, J., Troost, K., and de los Angeles, A., 2005, Serpent Spirit-power Stories along the Seattle Fault: Seism.Res.Lett., v.76.,4, 426-431.

Mai, P.M. and Beroza, G.C., 2002, A spatial random field model to characterize complexity in earthquake slip: J. Geophy. Res.: 107, No.B11, 2308.

Montgomery, D.R., Greenberge, H.M., Laprade, W.T., Nashem, W.D., 2001, Sliding in Seattle: test of a model of shallow landsliding potential in an urban environment. In: Wigmosta, M.S., Burges, S.J. (Eds), Land use and watersheds: Human influence on hydrology and geomorphology in urban and forest areas: Water Science and Application. American Geophysical Union, Washington, D.C., p59-73.

Moore, J.R., Gischig, V., Burjanek, J., Loew, S., and Fah, D., 2011, Site Effects in Unstable Rock Slopes: Dynamic Behavior of the Randa Instability (Switzerland): Bull. of Seism. Soc. of Am., v.101, 3110-3116.

Nelson, A.R., Johnson, S.Y., Kelsey, H.M., Wells, R.E., Sherrod, B.L., Pezzopane, S.K., Bradley, L-A., Koehler III. R.D. and Bucknam, R.C., 2003, Late Holocene earthquakes on the Toe Jam Hill fault, Seattle fault zone, Bainbridge Island, Washington: GSA Bulletin, v.114,no.11, 1388-1403.

Newmark, N.M., 1965, Effects of earthquakes on dams and embankments: Geotechnique, v.15, 139-160.

Noson, L.L., Qamar, A.I., and Thorsen, G.W., 1988, Washington State earthquake hazards: Olympia, Washington Division of Geology and Earth Resources Information Circular 85, 77 p.

Palmer, S.P., Magsino, S.L., Bilderback, E.L., Poelstra, J.L., Folger, D.S. and Niggemann, R.A., 2004, Liquefaction Susceptibility and Site Class Maps of Washington State, By County: WA DNR open file report 2004-20.

Paolucci, R., 2002, Amplification of earthquake ground motion by steep topographic irregularities: EQ Eng and Struct. Dyn., v.31, p,1831-1853.

Peng, W-F., Wang, C-L., Chen, S-T., and Lee, S-T., 2009a, A seismic landslide hazard analysis with topographic effect, a case study in the 99 Peaks region, Central Taiwan: Environ. Geol, v.57, p537-549.

Peng, W-F., Wang, C-L., Chen, S-T., and Lee, S-T., 2009b, Incorporating the effects of topographic amplification and sliding areas in the modeling of earthquake-induced landslide hazards, using the cumulative displacement method: Computers and Geosciences, v.35, p946-966.

Pratt, T.L., Johnson, S., Potter, C., Stephenson, W., Finn, C., 1997, Seismic reflection images beneath Puget Sound, western Washington State: The Puget Lowland thrust sheet hypothesis: J. Geophys. Res., v.102, p27,469-27,489.

Pratt, T.L., Brocher, T.M., Weaver, C.S., Creager, K.C., Snelson, C.M., Crosson, R.S., Miller, K.C. and Trehu, A.M., 2003, Amplification of Seismic Waves by the Seattle Basin, Washington State: Bull. of Seis. Soc. of Am., v.93, p533-545.

Pratt, T.L., and Brocher, T.M., 2006, Site Response and Attenuation in the Puget Lowland, Washington State: Bull. of Seis. Soc. of Am., v.96, p536-552.

Pringle, P.T., Schuster, R.L., Logan, R.L., 1998, New radiocarbon ages of major landslides in the Cascade Range, Washington: Washington Geology, v. 26, no. 1, p. 31-39; errata, Washington Geology, v. 26, no. 2/3, p. 69.

Sanchez-Sesma, F.J., 1985, Diffraction of Elastic SH Waves by Wedges: Bull. Seism. Soc. Am., 75:1435-1446.

Savage, W.Z., Morrissey, M.M. and R.L.Baum, 2000, Geotechnical Properties for Landslide-Prone Seattle-Area Glacial Deposits, U.S. Geological Survey, open file report 00-228, 5p.

Schuster, R.L., Logan, R.L. and Pringle, P.T., 1992, Prehistoric Rock Avalanches in the Olympic Mountains, Washington: Science, v.258, p.1620-1621.

Shahi, S.K., and Baker, J.W., 2010, An Empirically Calibrated Framework for Including the Effects of Near-Fault Directivity in Probabilistic Seismic Hazard Analysis: Bull. Seism. Soc. Am., 101:742-755.

Snelson, C.M., Brocher, T.M., Miller, K.C., Pratt, T.L. and Trehu, A.M., 2007, Seismic Amplification within the Seattle Basin, Washington State: Insights from SHIPS Seismic Tomography Experiments: Bull. of Seis. Soc. of Am., v.97, p1432-1448.

Steidl, J.H., Tumarkin, A.G., and Archuleta, R.J., 1996, What is a Reference Site?: Bull of Seism. Soc. of Am., 86, p.1733-1748.

Stein, S., and Wysession, M., 2003, An Introduction to Seismology, Earthquakes, and Earth Structure: Blackwell Publishing, Malden, MA.

Stewart, M., ed., 2005, Scenario for a Magnitude 6.7 Earthquake on the Seattle Fault: Earthquake Engineering Research Institute and Washington Military Department Emergency Management Division.

ten Brink, U.S., Song, J., and Bucknam, R.C., 2006, Rupture models for the A.D. 900-930 Seattle fault earthquake from uplifted shorelines: Geology, v.34, p.585-588.

Thorson, R. M., 1996, Earthquake recurrence and glacial loading in western Washington: Geological Society of America Bulletin, v. 108, p. 1182–1191.

Troost, Kathy Goetz, Booth, Derek B., Wisher, Aaron P., and Shimel, Scott A., 2005, The geologic map of Seattle - a progress report: U.S. Geological Survey Open-File Report 2005-1252

Tubbs, D.W., 1974, Landslides in Seattle, Dept. of Natural Resources division of geology and earth resources information circular no.52.

Wells, D. L., and Coppersmith, K. J., 1994, New empirical relationships among magnitude, rupture length, rupture width, rupture area, and surface displacement: Seismological Society of America Bulletin, v. 84, p. 974–1002.

Wieczorek, G.F.,Wilson, R.C., Harp, E.L., 1985, Map showing slope stability during earthquakes in San Mateo County - California. US Geol. Surv. Misc. Invest. Map I-1257-E,

Williams, R.A., Stephenson, W.J., Frankel, A.D., and Odum,J.K., 1999, Surface Seismic Measurements of Near-Surface P- and S-wave Seismic Velocities at Earthquake Recording Stations, Seattle, Washington, Earthquake Spectra, 15, No. 3.

Wong, I., Stokoe II, K.H., Cox, B.R., Lin, Y.-C. and Menq, F.-Y., 2010, Geotechnical Characterization and Evaluation of Site Amplification at Selected PNSN Strong Motion Sites, Seattle, Washington, Final Technical Report submitted to USGS under the National Earthquake Hazards Reduction Program. 38p.

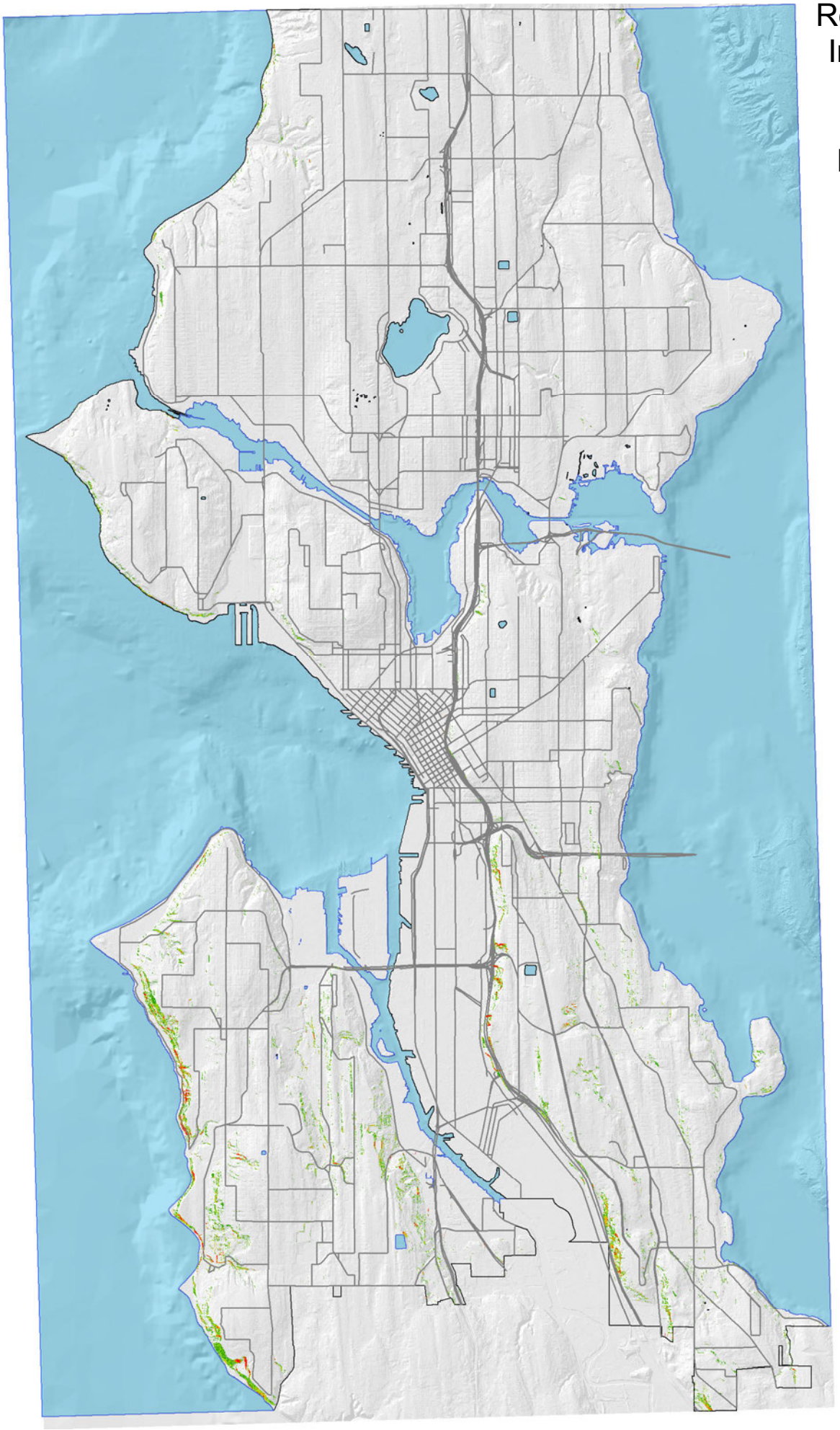

Relative Seismically Induced Landslide Hazard for Mw7 Seattle Fault Earthquake - Dry soil conditions

Relative Seismically Induced Landslide Hazard

Newmark displacement

- 1 - 5 cm - Low
- 5-15 cm - Moderate
- 15-30 cm - High
- >30 cm - Extremely High

0 0.5 1 2 Kilometers

N

Seismically Induced Landslide Hazard for Mw7 Seattle Fault Earthquake - Saturated soil conditions

Relative Seismically Induced Landslide Hazard

Newmark displacement

- 1 - 5 cm - Low
- 5-15 cm - Moderate
- 15-30 cm - High
- >30 cm - Extremely High

0 0.5 1 2 Kilometers

N

Depth to bottom (m)	Thickness (m)	Vs (m/s)	Dry density (kg/m^3)	Wet density (kg/m^3)	Description	Vs30 (m/s)
Unit 1 - 8m Qvt, 50m Qva, 30m Qvlc, Qpf						
1	1	150	1280	1536	soil	
3	2	400	1800	2160	Qvt	375
5	2	475	1875	2250	Qvt	
7	2	550	1950	2340	Qvt	
8	1	600	2000	2400	Qvt	
12	4	300	1600	1920	Qva	
17	5	350	1680	2016	Qva	
25	8	400	1700	2040	Qva	
35	10	450	1740	2088	Qva	
45	10	500	1760	2112	Qva	
50	5	550	1780	2136	Qva	
58	8	600	1800	2160	Qva	
68	10	400	1500	1800	Qvlc	
78	10	450	1550	1860	Qvlc	
83	5	500	1600	1920	Qvlc	
88	5	550	1650	1980	Qvlc	
	0	600	2000	2400	Qpf	
Unit 2 - 8m Qvt, 15m Qva, 20m Qvlc, Qpf						
1	1	150	1280	1536	soil	
3	2	400	1800	2160	Qvt	369
5	2	475	1875	2250	Qvt	
7	2	550	1950	2340	Qvt	
8	1	600	2000	2400	Qvt	
12	4	300	1740	2088	Qva	
17	5	350	1760	2112	Qva	
25	8	400	1700	2040	Qva	
35	10	400	1500	1800	Qvlc	
45	10	450	1550	1860	Qvlc	
	0	600	2000	2400	Qpf	
Unit 3 - 8m Qvt, 15m Qva, Qpf						
1	1	150	1280	1536	soil	
3	2	400	1800	2160	Qvt	421
5	2	475	1875	2250	Qvt	
7	2	550	1950	2340	Qvt	
8	1	600	2000	2400	Qvt	
16	8	350	1740	2088	Qva	
23	7	450	1760	2112	Qva	
	0	600	2000	2400	Qpf	
Unit 4 - 50m Qva, Qpf						
1	1	100	1280	1536	soil	
5	4	300	1600	1920	Qva	358
10	5	350	1680	2016	Qva	
18	8	400	1700	2040	Qva	
28	10	450	1740	2088	Qva	
38	10	500	1760	2112	Qva	
43	5	550	1780	2136	Qva	
	0	600	1800	2160	Qva	
Unit 5 - 25m Qva, Qpf						
1	1	100	1280	1536	soil	368
5	4	300	1600	1920	Qva	
10	5	350	1680	2016	Qva	
18	8	400	1700	2040	Qva	
25	7	450	1740	2088	Qva	
	0	600	2000	2400	Qpf	
Unit 6 - 10m Qva, Qpf						
1	1	100	1280	1536	soil	403
5	4	300	1600	1920	Qva	
10	5	350	1680	2016	Qva	
15	5	450	1800	2160	Qpf	
20	5	550	1900	2280	Qpf	
	0	600	2000	2400	Qpf	
Unit 7 - 50m Qva, 30m Qvlc, Qpf						
1	1	100	1280	1536	soil	358
5	4	300	1600	1920	Qva	
10	5	350	1680	2016	Qva	
18	8	400	1700	2040	Qva	
28	10	450	1740	2088	Qva	
38	10	500	1760	2112	Qva	
43	5	550	1780	2136	Qva	
50	7	600	1800	2160	Qva	
60	10	400	1500	1800	Qvlc	
70	10	450	1550	1860	Qvlc	

Depth to bottom (m)	Thickness (m)	Vs (m/s)	Dry density (kg/m^3)	Wet density (kg/m^3)	Description	Vs30 (m/s)
80	10	500	1600	1920	Qvlc	
	0	600	2000	2400	Qpf	
Unit 8 - 25m Qva, 25m Qvlc, Qpf						
1	1	100	1280	1536	soil	350
5	4	300	1600	1920	Qva	
10	5	350	1680	2016	Qva	
18	8	400	1700	2040	Qva	
25	7	450	1740	2088	Qva	
35	10	400	1500	1800	Qvlc	
45	10	450	1550	1860	Qvlc	
50	5	500	1600	1920	Qvlc	
	0	600	2000	2400	Qpf	
Unit 9 - 10m Qva, 30m Qvlc, Qpf						
1	1	100	1280	1536	soil	301
5	4	300	1600	1920	Qva	
10	5	350	1680	2016	Qva	
20	10	300	1300	1560	Qvlc	
30	10	350	1400	1680	Qvlc	
40	10	400	1500	1800	Qvlc	
	0	600	2000	2400	Qpf	
Unit 10 - 5m Qvr, 25m Qvlc, Qpf						
1	1	100	1280	1536	soil	
3	2	250	1450	1740	Qvr	230
5	2	350	1500	1800	Qvr	
15	10	200	1300	1560	Qvlc	
25	10	250	1350	1620	Qvlc	
30	5	300	1400	1680	Qvlc	
	0	600	2000	2400	Qpf	
Unit 11 - 30m Qvlc, Qpf						
1	1	100	1280	1536	soil	234
11	10	200	1300	1560	Qvlc	
21	10	250	1350	1620	Qvlc	
26	5	300	1400	1680	Qvlc	
31	5	350	1500	1800	Qvlc	
	0	600	2000	2400	Qpf	
Unit 12 - 15m Qvlc, Qpf						
1	1	100	1280	1536	soil	281
11	10	200	1300	1560	Qvlc	
16	5	250	1350	1620	Qvlc	
21	5	450	1800	2160	Qpf	
26	5	550	1900	2280	Qpf	
	0	600	2000	2400	Qpf	
Unit 13 - 5m Qvr, 8m Qvt, 50m Qva, 30m Qvlc, Qpf						
1	1	100	1280	1536	soil	368
3	2	250	1450	1740	Qvr	
5	2	350	1500	1800	Qvr	
7	2	400	1800	2160	Qvt	
9	2	475	1875	2250	Qvt	
11	2	550	1950	2340	Qvt	
13	2	600	2000	2400	Qvt	
17	4	350	1680	2016	Qva	
22	5	400	1700	2040	Qva	
30	8	450	1740	2088	Qva	
40	10	500	1760	2112	Qva	
50	10	550	1780	2136	Qva	
55	5	600	1800	2160	Qva	
	0	600	1800	2160	Qva	
Unit 14 - 5m Qvr, 8m Qvt, 20m Qva, 25m Qvlc, Qpf						
1	1	100	1280	1536	soil	368
3	2	250	1450	1740	Qvr	
5	2	350	1500	1800	Qvr	
7	2	400	1800	2160	Qvt	
9	2	475	1875	2250	Qvt	
11	2	550	1950	2340	Qvt	
13	2	600	2000	2400	Qvt	
17	4	350	1680	2016	Qva	
22	5	400	1700	2040	Qva	
30	8	450	1740	2088	Qva	
39	9	500	1760	2112	Qva	
49	10	400	1500	1800	Qvlc	
59	10	450	1550	1860	Qvlc	
64	5	500	1600	1920	Qvlc	
	0	600	2000	2400	Qpf	

Depth to bottom (m)	Thickness (m)	Vs (m/s)	Dry density (kg/m^3)	Wet density (kg/m^3)	Description	Vs30 (m/s)
Unit 15 - 5m Qvr, 8m Qvt, 15m Qva, Qpf						
1	1	100	1280	1536	soil	373
3	2	250	1450	1740	Qvr	
5	2	350	1500	1800	Qvr	
7	2	400	1800	2160	Qvt	
9	2	475	1875	2250	Qvt	
11	2	550	1950	2340	Qvt	
13	2	600	2000	2400	Qvt	
17	4	350	1680	2016	Qva	
22	5	400	1700	2040	Qva	
28	6	450	1740	2088	Qva	
	0	600	2000	2400	Qpf	
Unit 16 - 5m Qvr, 50m Qva, 30m Qvlc, Qpf						
1	1	100	1280	1536	soil	
3	2	250	1450	1740	Qvr	420
5	2	350	1500	1800	Qvr	
9	4	350	1680	2016	Qva	
14	5	400	1700	2040	Qva	
22	8	450	1740	2088	Qva	
32	10	500	1760	2112	Qva	
42	10	550	1780	2136	Qva	
47	5	600	1800	2160	Qva	
52	5	600	1800	2160	Qva	
62	10	400	1500	1800	Qvlc	
72	10	450	1550	1860	Qvlc	
77	5	500	1600	1920	Qvlc	
	0	600	2000	2400	Qpf	
Unit 17 - 5m Qvr, 15m Qva, 25m Qvlc, Qpf						
1	1	100	1280	1536	soil	
3	2	250	1450	1740	Qvr	349
5	2	350	1500	1800	Qvr	
9	4	350	1680	2016	Qva	
14	5	400	1700	2040	Qva	
20	6	450	1740	2088	Qva	
30	10	400	1500	1560	Qvlc	
40	10	450	1550	1620	Qvlc	
45	5	300	1400	1680	Qvlc	
	0	600	2000	2400	Qpf	
Unit 18 - 5m Qvr, 15m Qva, Qpf						
1	1	100	1280	1536	soil	386
3	2	250	1450	1740	Qvr	
5	2	350	1500	1800	Qvr	
9	4	350	1680	2016	Qva	
14	5	400	1700	2040	Qva	
20	6	450	1740	2088	Qva	
	0	600	2000	2400	Qpf	
Unit 19 - 10m Qp, Qpf						
10	10	60	1050	1260	Peat	147
15	5	450	1800	2160	Qpf	
20	5	550	1900	2280	Qpf	
	0	600	2000	2400	Qpf	
Unit 20 - 5m Fill, 8m Qvt, 50m Qva, 30m Qvlc, Qpf						
1	1	100	1200	1440	soil	283
3	2	120	1200	1440	Fill	
5	2	130	1200	1440	Fill	
7	2	400	1800	2160	Qvt	
9	2	475	1875	2250	Qvt	
11	2	550	1950	2340	Qvt	
13	2	600	2000	2400	Qvt	
17	4	300	1600	1920	Qva	
22	5	350	1680	2016	Qva	
30	8	400	1700	2040	Qva	
40	10	450	1740	2088	Qva	
50	10	500	1760	2112	Qva	
55	5	550	1780	2136	Qva	
63	8	600	1800	2160	Qva	
73	10	400	1500	1800	Qvlc	
83	10	450	1550	1860	Qvlc	
88	5	500	1600	1920	Qvlc	
93	5	550	1650	1980	Qvlc	
	0	600	2000	2400	Qpf	
Unit 21 - 6m Qt/Qal,8m Qvt, 50m Qva, 30m Qvlc, Qpf						
1	1	100	1200	1440	soil	259

Depth to bottom (m)	Thickness (m)	Vs (m/s)	Dry density (kg/m^3)	Wet density (kg/m^3)	Description	Vs30 (m/s)
3	2	120	1200	1440	Qt/Qal	
6	3	130	1200	1440	Qt/Qal	
8	2	400	1800	2160	Qvt	
10	2	475	1875	2250	Qvt	
12	2	550	1950	2340	Qvt	
14	2	600	2000	2400	Qvt	
18	4	300	1600	1920	Qva	
23	5	350	1680	2016	Qva	
31	8	400	1700	2040	Qva	
41	10	450	1740	2088	Qva	
51	10	500	1760	2112	Qva	
56	5	550	1780	2136	Qva	
64	8	600	1800	2160	Qva	
74	10	400	1500	1800	Qvlc	
84	10	450	1550	1860	Qvlc	
89	5	500	1600	1920	Qvlc	
94	5	550	1650	1980	Qvlc	
	0	600	2000	2400	Qpf	
Unit 22 - 10m Qls, Qpf						
1	1	100	1200	1440	soil	262
3	2	120	1200	1440	Landslide	
5	2	130	1200	1440	Landslide	
10	5	140	1250	1500	Landslide	
15	5	450	1800	2160	Qpf	
20	5	550	1900	2280	Qpf	
	0	600	2000	2400	Qpf	
Unit 23 - 5m Qls, Qpf						
1	1	100	1200	1440	soil	344
3	2	120	1200	1440	Landslide	
5	2	130	1200	1440	Landslide	
10	5	450	1800	2160	Qpf	
15	5	550	1900	2280	Qpf	
	0	600	2000	2400	Qpf	
Unit 24 - 3m Qls, 25m Qvlc, Qpf						
1	1	100	1200	1440	soil	220
3	2	120	1200	1440	Landslide	
13	10	200	1300	1560	Qvlc	
23	10	250	1350	1620	Qvlc	
28	5	300	1400	1680	Qvlc	
	0	600	2000	2400	Qpf	
Unit 25 - 3m Qls, 15m Qva, 25m Qvlc, Qpf						
1	1	100	1200	1440	soil	289
3	2	120	1200	1440	Landslide	
13	10	300	1600	1920	Qva	
18	5	350	1680	2016	Qva	
26	8	400	1700	2040	Qva	
28	2	450	1740	2088	Qva	
38	10	400	1500	1800	Qvlc	
48	10	450	1550	1860	Qvlc	
53	5	500	1600	1920	Qvlc	
	0	600	2000	2400	Qpf	
Unit 26 - 10m Fill, 5m Qvr, Qpf						
1	1	100	1200	1440	soil	244
3	2	120	1200	1440	Fill	
5	2	130	1200	1440	Fill	
10	5	140	1250	1500	Fill	
12	2	250	1400	1680	Qvr	
15	3	350	1500	1800	Qvr	
20	5	450	1800	2160	Qpf	
25	5	550	1900	2280	Qpf	
	0	600	2000	2400	Qpf	
Unit 27 - 10m Fill, Qpf						
1	1	100	1200	1440	soil	262
3	2	120	1200	1440	Fill	
5	2	130	1200	1440	Fill	
10	5	140	1250	1500	Fill	
15	5	450	1800	2160	Qpf	
20	5	550	1900	2280	Qpf	
	0	600	2000	2400	Qpf	
Unit 28 - 10m Fill, 50m Qtf, Qpf						
1	1	100	1200	1440	soil	130
3	2	120	1200	1440	Fill	
5	2	130	1200	1440	Fill	

Depth to bottom (m)	Thickness (m)	Vs (m/s)	Dry density (kg/m^3)	Wet density (kg/m^3)	Description	Vs30 (m/s)
10	5	140	1250	1500	Fill	
30	20	130	1280	1536	Qtf	
60	30	170	1300	1560	Qtf	
	0	600	2000	2400	Qpf	
Unit 29-31 - 4m Fill, 30m Qal, Qva (Duwamish area)						
2	2	100	1200	1440	Fill	142
4	2	110	1200	1440	Fill	
9	5	125	1200	1440	Qal	
14	5	135	1200	1440	Qal	
24	10	160	1300	1560	Qal	
34	10	180	1350	1620	Qal	
38	4	300	1600	1920	Qva	
43	5	350	1680	2016	Qva	
51	8	400	1700	2040	Qva	
61	10	450	1740	2088	Qva	
71	10	500	1760	2112	Qva	
76	5	550	1780	2136	Qva	
	0	600	1800	2160	Qva	
Unit 32 - 3m Fill, 8m Qvt, 50m Qva, 30m Qvlc, Qpf						
1	1	100	1200	1440	soil	316
3	2	120	1200	1440	Fill	
5	2	400	1800	2160	Qvt	
7	2	475	1875	2250	Qvt	
9	2	550	1950	2340	Qvt	
11	2	600	2000	2400	Qvt	
15	4	300	1600	1920	Qva	
20	5	350	1680	2016	Qva	
28	8	400	1700	2040	Qva	
38	10	450	1740	2088	Qva	
48	10	500	1760	2112	Qva	
53	5	550	1780	2136	Qva	
61	8	600	1800	2160	Qva	
71	10	400	1500	1800	Qvlc	
81	10	450	1550	1860	Qvlc	
86	5	500	1600	1920	Qvlc	
91	5	550	1650	1980	Qvlc	
	0	600	2000	2400	Qpf	
Unit 33 - 5m Fill, 5m Qvr, 8m Qvt, 50m Qva, 30m Qvlc, Qpf						
1	1	100	1200	1440	soil	273
3	2	120	1200	1440	Fill	
5	2	130	1200	1440	Fill	
7	2	250	1400	1680	Qvr	
10	3	350	1500	1800	Qvr	
12	2	400	1800	2160	Qvt	
14	2	475	1875	2250	Qvt	
16	2	550	1950	2340	Qvt	
18	2	600	2000	2400	Qvt	
22	4	300	1600	1920	Qva	
27	5	350	1680	2016	Qva	
35	8	400	1700	2040	Qva	
45	10	450	1740	2088	Qva	
55	10	500	1760	2112	Qva	
60	5	550	1780	2136	Qva	
68	8	600	1800	2160	Qva	
78	10	400	1500	1800	Qvlc	
88	10	450	1550	1860	Qvlc	
93	5	500	1600	1920	Qvlc	
98	5	550	1650	1980	Qvlc	
	0	600	2000	2400	Qpf	
Unit 34 - 6m Qt/Qal, Qpf						
1	1	100	1200	1440	soil	322
3	2	120	1200	1440	Qt/Qal	
6	3	130	1200	1440	Qt/Qal	
11	5	450	1800	2160	Qpf	
16	5	550	1900	2280	Qpf	
	0	600	2000	2400	Qpf	
Unit 35 - 3m Fill, 50m Qva, 30m Qvlc, Qpf						
1	1	100	1200	1440	soil	311
3	2	120	1200	1440	Fill	
7	4	300	1600	1920	Qva	
12	5	350	1680	2016	Qva	
20	8	400	1700	2040	Qva	
30	10	450	1740	2088	Qva	
40	10	500	1760	2112	Qva	
45	5	550	1780	2136	Qva	

Depth to bottom (m)	Thickness (m)	Vs (m/s)	Dry density (kg/m^3)	Wet density (kg/m^3)	Description	Vs30 (m/s)
53	8	600	1800	2160	Qva	
63	10	400	1500	1800	Qvlc	
73	10	450	1550	1860	Qvlc	
78	5	500	1600	1920	Qvlc	
83	5	550	1650	1980	Qvlc	
	0	600	2000	2400	Qpf	
Unit 36 - Qpf						
1	1	100	1280	1536	soil	485
6	5	450	1800	2160	Qpf	
11	5	550	1900	2280	Qpf	
	0	600	2000	2400	Qpf	
Unit 37 - 5m Qvr, Qpf						
1	1	100	1280	1536	soil	435
3	2	250	1450	1740	Qvr	
5	2	350	1500	1800	Qvr	
10	5	450	1800	2160	Qpf	
15	5	550	1900	2280	Qpf	
	0	600	2000	2400	Qpf	
Unit 39 - 8m Qvt, 50m Qva, Qpf						
1	1	150	1280	1536	soil	
3	2	400	1800	2160	Qvt	413
5	2	475	1875	2250	Qvt	
7	2	550	1950	2340	Qvt	
8	1	600	2000	2400	Qvt	
16	8	350	1740	2088	Qva	
24	8	450	1760	2112	Qva	
32	8	550	1780	2136	Qva	
	0	600	1800	2160	Qva	
Unit 40 - 8m Qvt, 15m Qva, Qpf (identical to Unit 3)						
1	1	150	1280	1536	soil	
3	2	400	1800	2160	Qvt	421
5	2	475	1875	2250	Qvt	
7	2	550	1950	2340	Qvt	
8	1	600	2000	2400	Qvt	
16	8	350	1740	2088	Qva	
23	7	450	1760	2112	Qva	
	0	600	2000	2400	Qpf	
Unit 41 - 8m Qvt, 30m Qva, 20m Qvlc, Qpf						
1	1	150	1280	1536	soil	
3	2	400	1800	2160	Qvt	413
5	2	475	1875	2250	Qvt	
7	2	550	1950	2340	Qvt	
8	1	600	2000	2400	Qvt	
16	8	350	1740	2088	Qva	
24	8	450	1760	2112	Qva	
32	8	550	1780	2136	Qva	
38	6	600	1800	2160	Qva	
48	10	400	1500	1800	Qvlc	
58	10	450	1550	1860	Qvlc	
	0	600	2000	2400	Qpf	
Unit 42 - 8m Qvt, 15m Qva, Qpf						
1	1	150	1280	1536	soil	421
3	2	400	1800	2160	Qvt	
5	2	475	1875	2250	Qvt	
7	2	550	1950	2340	Qvt	
8	1	600	2000	2400	Qvt	
16	8	350	1740	2088	Qva	
23	7	450	1760	2112	Qva	
	0	600	2000	2400	Qpf	
Unit 43 - 8m Qvt, Qpf						
1	1	150	1280	1536	soil	489
3	2	400	1800	2160	Qvt	
5	2	475	1875	2250	Qvt	
7	2	550	1950	2340	Qvt	
8	1	600	2000	2400	Qvt	
13	5	450	1800	2160	Qpf	
18	5	550	1900	2280	Qpf	
	0	600	2000	2400	Qpf	
Unit 44 - 5m Fill, 5m Qvr, Qpf						
1	1	100	1200	1440	soil	314
3	2	120	1200	1440	Fill	
5	2	130	1200	1440	Fill	

Depth to bottom (m)	Thickness (m)	Vs (m/s)	Dry density (kg/m^3)	Wet density (kg/m^3)	Description	Vs30 (m/s)
7	2	250	1450	1740	Qvr	
10	3	350	1500	1800	Qvr	
15	5	450	1800	2160	Qpf	
20	5	550	1900	2280	Qpf	
	0	600	2000	2400	Qpf	
Unit 45 - 5m Fill, 5m Qal, Qpf						
1	1	100	1200	1440	soil	253
3	2	120	1200	1440	Fill	
5	2	130	1200	1440	Fill	
7	2	120	1200	1440	Qt/Qal	
10	3	130	1200	1440	Qt/Qal	
15	5	450	1800	2160	Qpf	
20	5	550	1900	2280	Qpf	
	0	600	2000	2400	Qpf	
Unit 46 - 5m Fill, 5m Qvt, Qpf						
1	1	100	1200	1440	soil	334
3	2	120	1200	1440	Fill	
5	2	130	1200	1440	Fill	
7	2	400	1800	2160	Qvt	
9	2	475	1875	2250	Qvt	
10	1	550	1950	2340	Qvt	
15	5	450	1800	2160	Qpf	
20	5	550	1900	2280	Qpf	
	0	600	2000	2400	Qpf	
Unit 47 - 5m Qvr, 8m Qvt, 15m Qva, Qpf						
1	1	100	1280	1536	soil	373
3	2	250	1450	1740	Qvr	
5	2	350	1500	1800	Qvr	
7	2	400	1800	2160	Qvt	
9	2	475	1875	2250	Qvt	
11	2	550	1950	2340	Qvt	
13	2	600	2000	2400	Qvt	
17	4	350	1680	2016	Qva	
22	5	400	1700	2040	Qva	
28	6	450	1740	2088	Qva	
	0	600	2000	2400	Qpf	
Unit 48 - 3m Qls, 15m Qva, Qpf						
1	1	100	1200	1440	soil	323
3	2	120	1200	1440	Landslide	
7	4	300	1600	1920	Qva	
12	5	350	1680	2016	Qva	
18	6	400	1700	2040	Qva	
23	5	450	1800	2160	Qpf	
28	5	550	1900	2280	Qpf	
	0	600	2000	2400	Qpf	
Unit 49 - 3m Qls, 5m Qvr, Qpf						
1	1	100	1200	1440	soil	360
3	2	120	1200	1440	Landslide	
5	2	250	1450	1740	Qvr	
8	3	350	1500	1800	Qvr	
13	5	450	1800	2160	Qpf	
18	5	550	1900	2280	Qpf	
	0	600	2000	2400	Qpf	
Unit 50 - 5m alluvium, Qpf						
1	1	100	1200	1440	soil	344
3	2	120	1200	1440	Qt/Qal	
5	2	130	1200	1440	Qt/Qal	
10	5	450	1800	2160	Qpf	
15	5	550	1900	2280	Qpf	
	0	600	2000	2400	Qpf	
Unit 51 - 8m Qb, Qpf						
2	2	120	1200	1440	Beach	298
4	2	130	1200	1440	Beach	
8	4	140	1250	1500	Beach	
13	5	450	1800	2160	Qpf	
18	5	550	1900	2280	Qpf	
	0	600	2000	2400	Qpf	
Unit 52 - 3m Ql, Qpf						
2	2	130	1300	1560	Ql	425
3	1	150	1400	1680	Ql	
8	5	450	1800	2160	Qpf	
13	5	550	1900	2280	Qpf	

Depth to bottom (m)	Thickness (m)	Vs (m/s)	Dry density (kg/m^3)	Wet density (kg/m^3)	Description	Vs30 (m/s)
	0	600	2000	2400	Qpf	
Unit 53 - 2m Fill, 3m Ql,Qpf						
2	2	120	1200	1440	Fill	357
4	2	130	1300	1560	Ql	
5	1	150	1400	1680	Ql	
10	5	450	1800	2160	Qpf	
15	5	550	1900	2280	Qpf	
	0	600	2000	2400	Qpf	
Unit 54 - 3m Qls, 30m Qva, 25m Qvlc, Qpf						
1	1	100	1200	1440	soil	311
3	2	120	1200	1440	Landslide	
7	4	300	1600	1920	Qva	
12	5	350	1680	2016	Qva	
20	8	400	1700	2040	Qva	
30	10	450	1740	2088	Qva	
33	3	500	1760	2112	Qva	
43	10	400	1500	1800	Qvlc	
53	10	450	1550	1860	Qvlc	
58	5	500	1600	1920	Qvlc	
	0	600	2000	2400	Qpf	
Unit 55 -Tb						
2	2	350	1920	2304	Weathered rock	552
4	2	400	1950	2340	Weathered rock	
5	1	500	1970	2364	Weathered rock	
	0	600	2000	2400	Tb or other rock	
Unit 56 - 3m Qls, Tb						
1	1	100	1200	1440	soil	394
3	2	120	1200	1440	Landslide	
5	2	350	1920	2304	Crap	
7	2	400	1950	2340	Crap	
8	1	500	1970	2364	Crap	
	0	600	2000	2400	Tb or other rock	
Unit 57 - 6m Fill, Tb						
1	1	100	1200	1440	soil	321
3	2	120	1200	1440	Fill	
5	2	130	1200	1440	Fill	
6	1	140	1250	1500	Fill	
8	2	350	1920	2304	Crap	
10	2	400	1950	2340	Crap	
11	1	500	1970	2364	Crap	
	0	600	2000	2400	Tb or other rock	
Unit 58 - 8m Qvt, Tb						
1	1	100	1200	1440	soil	490
3	2	400	1800	2160	Qvt	
5	2	475	1875	2250	Qvt	
7	2	550	1950	2340	Qvt	
8	1	600	2000	2400	Qvt	
	0	600	2000	2400	Tb or other rock	
Unit 59 - 3m Qls, 8m Qvt, Tb						
1	1	100	1200	1440	soil	403
3	2	120	1200	1440	Landslide	
5	2	400	1800	2160	Qvt	
7	2	475	1875	2250	Qvt	
9	2	550	1950	2340	Qvt	
11	2	600	2000	2400	Qvt	
	0	600	2000	2400	Tb or other rock	
Unit 60 - 8m Qb,Tb						
2	2	120	1200	1440	Beach	295
4	2	130	1200	1440	Beach	
8	4	140	1250	1500	Beach	
10	2	350	1920	2304	Weathered rock	
12	2	400	1950	2340	Weathered rock	
13	1	500	1970	2364	Weathered rock	
	0	600	2000	2400	Tb or other rock	
Unit 61 - 8m Qvt, 30m Qvlc, Qpf						
1	1	100	1200	1440	soil	251
3	2	400	1800	2160	Qvt	
5	2	475	1875	2250	Qvt	
7	2	550	1950	2340	Qvt	
9	2	600	2000	2400	Qvt	
19	10	200	1300	1560	Qvlc	

Depth to bottom (m)	Thickness (m)	Vs (m/s)	Dry density (kg/m^3)	Wet density (kg/m^3)	Description	Vs30 (m/s)
29	10	250	1350	1620	Qvlc	
34	5	300	1400	1680	Qvlc	
39	5	350	1500	1800	Qvlc	
	0	600	2000	2400	Qpf	
Unit 62 - 5m Qvrl, 15m Qva, 25m Qvlc, Qpf						
1	1	100	1200	1440	soil	327
3	2	250	1450	1740	Qvrl	
6	3	350	1500	1800	Qvrl	
10	4	300	1600	1920	Qva	
15	5	350	1680	2016	Qva	
21	6	400	1700	2040	Qva	
31	10	400	1500	1800	Qvlc	
41	10	450	1550	1860	Qvlc	
46	5	500	1600	1920	Qvlc	
	0	600	2000	2400	Qpf	
Unit 63 - 2m fill, 13m Qvrl, Qpf						
1	1	100	1200	1440	soil	382
2	1	120	1200	1440	Fill	
4	2	250	1450	1740	Qvrl	
7	3	350	1500	1800	Qvrl	
10	3	400	1600	1920	Qvrl	
15	5	450	1650	1980	Qvrl	
	0	600	2000	2400	Qpf	
Unit 64 - 5m Qvrl, Qpf or Tb						
1	1	100	1200	1440	soil	435
3	2	250	1450	1740	Qvrl	
5	2	350	1500	1800	Qvrl	
10	5	450	1800	2160	Qpf/Tb	
15	5	550	1900	2280	Qpf/Tb	
	0	600	2000	2400	Qpf/Tb	
Unit 65 - 8m Qvt, 30m Qvlc, Qpf						
1	1	100	1200	1440	soil	251
3	2	400	1800	2160	Qvt	
5	2	475	1875	2250	Qvt	
7	2	550	1950	2340	Qvt	
9	2	600	2000	2400	Qvt	
19	10	200	1300	1560	Qvlc	
29	10	250	1350	1620	Qvlc	
34	5	300	1400	1680	Qvlc	
39	5	350	1500	1800	Qvlc	
	0	600	2000	2400	Qpf	
Unit 66 - 3m Fill, 8m Qvt, 20m Qva, Qpf						
1	1	100	1200	1440	soil	316
3	2	120	1200	1440	Fill	
5	2	400	1800	2160	Qvt	
7	2	475	1875	2250	Qvt	
9	2	550	1950	2340	Qvt	
11	2	600	2000	2400	Qvt	
15	4	300	1600	1920	Qva	
20	5	350	1680	2016	Qva	
28	8	400	1700	2040	Qva	
31	3	450	1740	2088	Qva	
	0	600	2000	2400	Qpf	
Unit 67 - 5m Qvr, Tb						
2	2	250	1450	1740	Qvr	479
5	3	350	1500	1800	Qvr	
7	2	350	1920	2304	Weathered rock	
9	2	400	1950	2340	Weathered rock	
10	1	500	1970	2364	Weathered rock	
	0	600	2000	2400	Tb or other rock	